Impact of climate change on VRE lulls

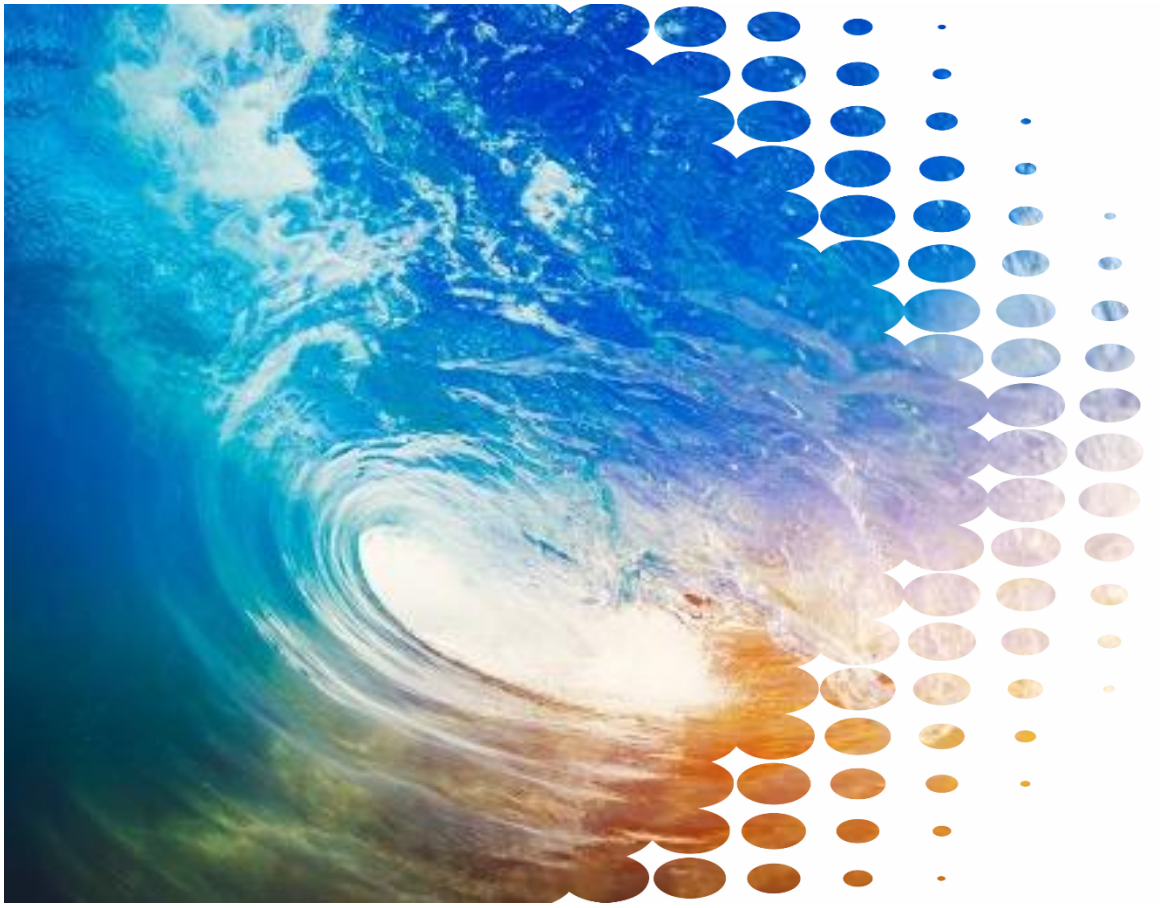

ASL

August 2025

RISK FRONTIERS

Risk Frontiers Disclaimer

This report incorporates the use of data and mathematical and empirical models developed using and including third party data and models. Any and all data, results and other information contained within this report ("Results") are subject to certain inherent limitations including potential errors in the models/ data, shortcomings in the experiment designs, the conjectural quality of the forcing scenarios used to drive the models and statistical uncertainty of model results. While this report has been prepared in good faith, the Results are inherently uncertain (particularly with respect to forward looking matters) and it is not possible within the context and scope of this report to verify the accuracy and completeness of the Results. Accordingly, this report is provided on an "as is" basis. To the maximum extent permitted by law, Risk Frontiers excludes all express or implied representations or warranties related to this report, including, but not limited to, warranties of accuracy, completeness, reliability, merchantability and fitness for a particular purpose. The reliance that the user places on this report, and the Results, is a matter for its own judgment.

Table of Contents

Introduction

ASL publishes a biennial Infrastructure Investment Objectives (IIO) report which sets out the 20-year development pathway of generation, long duration storage and firming infrastructure for NSW. The IIO report must contain an assessment of the resilience of the NSW electricity system in relation to lulls in Variable Renewable Energy (VRE) sources, as it relates to the development pathway in the report, including by reference to climate modelling – EII s45(4) / Regulations 24(2)(e). VRE lulls have been assessed in previous IIO reports in 2022 and 2023 (see Appendix 1). This report expands on previous work by incorporating climate modelling into the assessment process.

The primary focus of the 2025 approach is to understand the magnitude of any projected changes to VRE lull frequency and duration across all Renewable Energy Zones (REZ) in the National Electricity Market (NEM). It builds on existing research which has investigated present day climatology of VRE lulls (OECC, 2023; Richardson et al., 2023) and utilises recent advancements in Australian weather and climate data.

This report describes the methodology and results of the analysis undertaken by Risk Frontiers on historical and projected VRE lulls across the NEM. This analysis enabled ASL to assess the resilience of the NSW electricity system to the VRE lulls observed in the climate projections. The results of both the VRE lull analysis and the resilience assessment are presented in the 2025 IIO report.

Approach

The 2025 approach consists of two parts. Part 1 is a bottom-up approach that seeks to understand the impact of climate change on VRE resource available. This section looks at projected changes in the frequency and duration of lulls in wind and solar energy availability, independent of planned capacity under the development pathway. Part 2 is a top-down approach that identifies the distribution of VRE lull duration with consideration of climate model projections and the capacity expansion plan. This allows ASL to conduct their resilience assessment by simulating their development pathway against these lulls.

Data sources

Weather and climate analyses in the 2025 approach are based on the latest generation of gridded historical weather observations and regional climate model (RCM) simulations of possible future scenarios.

Historical VRE lulls are identified from the Bureau of Meteorology Atmospheric high-resolution Regional Reanalysis for Australia – Convective Scale Version 2 (BARRA-C2). BARRA-C2 is a kilometre-scale (4.4 km) downscaled reanalysis over Australia and covers the period from 1979 to present. Although it has not yet been comprehensively evaluated, it is expected to provide a substantial improvement over previous datasets for Australian applications (Chun-Hsu et. al., 2022).

Possible future VRE lulls are identified from the Bureau of Meteorology Atmospheric Regional Projections for Australia - Regional (BARPA-R). BARPA-R provides moderate-resolution (17 km) regional climate projections over Australia and the surrounding regions. The BARPA ensemble consists of 7 driving models and 2 scenarios. All regional climate model data used in this study are bias corrected to BARRA-C2 using quantile mapping. Further information on CMIP6 scenarios, regional climate modelling for Australia, and bias correction are provided in Appendix 2.

Part 1: Bottom-up VRE lulls forecasting

The objective of Part 1 is to understand the likely impact of climate change on the frequency and severity of VRE lulls. Key objectives of the bottom-up approach include:

- To use BARPA RCM climate forecast dataset, at a daily data resolution, calibrated to BARRA-C2 reanalysis data.
- To define VRE lulls as periods where 3-day running average NEM-wide wind speed or solar irradiance falls below the 5th percentile of NEM-wide data. This analysis is an extension of existing literature conducted by Richardson et al. (2023).
- To analyse frequency and duration of NEM-wide wind, solar and compound VRE lulls.
- To analyse trends across time (including historical observations and future climate scenarios) and seasons.
- To analyse temperature profiles during VRE lulls.
- To analyse RCM projections for rainfall and drought at hydroelectric dams.
- To analyse climatic drivers of VRE lulls.

Part 2: Top-down VRE lulls assessment

The objective of Part 2 is to identify the distribution of possible future VRE lull durations from climate model projections with consideration for the capacity expansion plan across a range of future time periods. Key objectives of the top-down approach include:

- To overlay the projected electricity infrastructure as modelled in the IIO report by weighting wind speeds and solar irradiance data by capacity of wind/solar across REZs.
- To identify a range of challenging VRE lulls from select forecast years.

The identified VRE lulls were then simulated by ASL in time-sequential modelling. This allowed ASL to assess the resilience of the NSW electricity system to VRE lulls in their 2025 IIO.

Part 1: Bottom-up Approach

The bottom-up approach investigates the weather and climate associated with NEM-wide VRE lulls and how this may change under plausible global warming scenarios. Understanding how climate change may affect resource availability at future time periods can help to explain any changes in event frequency and severity, observed in Part 2: top-down approach.

Renewable Energy Zones across the National Electricity Market

For the Part 1 bottom-up approach, analysis is restricted to key REZs across the NEM, where included REZs have > 500 MW capacity of wind or solar by 2045 in at least one scenario from the 2025 IIO Ambition and Supply Chain Constrained scenarios or the 2024 ISP Step Change and Progressive Change scenarios (Figure 1). By excluding REZs with less than 500 MW, the analysis is limited to 30 wind and/or solar REZ.

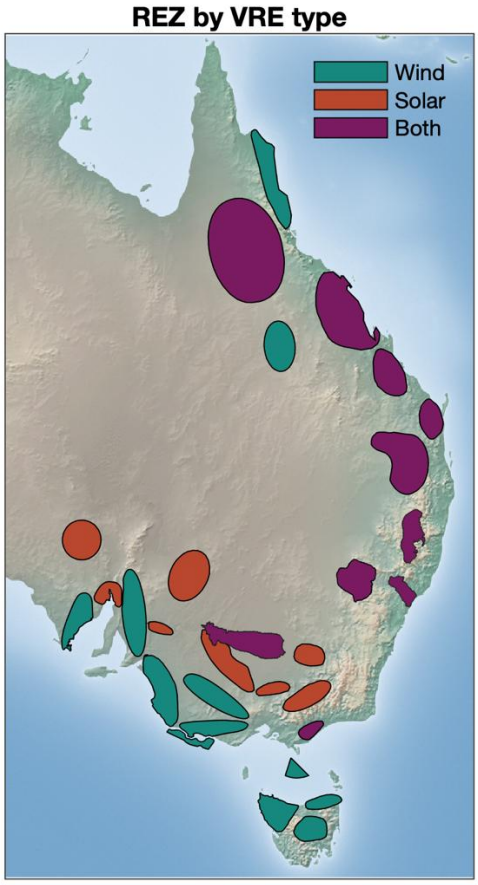

REZ ID	REZ name	Wind	Solar
Q1	Far North QLD	Include	Exclude
Q2	North Qld Clean Energy Hub	Include	Include
Q3	Northern Qld	Exclude	Exclude
Q4	Isaac	Include	Include
Q5	Barcaldine	Include	Exclude
Q6	Fitzroy	Include	Include
Q7	Wide Bay	Include	Include
Q8	Darling Downs	Include	Include
Q9	Banana	Exclude	Exclude
N1	North West NSW	Exclude	Exclude
N2	New England	Include	Include
N3	Central-West Orana	Include	Include
N4	Broken Hill	Exclude	Include
N5	South West NSW	Include	Include
N6	Wagga Wagga	Exclude	Include
N7	Tumut	Exclude	Exclude
N8	Cooma-Monaro	Exclude	Exclude
N9	Hunter-Central Coast	Include	Include
N10	Hunter Coast	Exclude	Exclude
N11	Illawarra Coast	Exclude	Exclude
N12	Illawarra	Exclude	Exclude
V1	Ovens Murray	Exclude	Include
V2	Murray River	Exclude	Include
V3	Western Victoria	Include	Exclude
V4	South West Victoria	Include	Exclude
V5	Gippsland	Include	Include
V6	Central North Vic	Exclude	Include
V7	Gippsland Coast	Include	Exclude
V8	Southern Ocean (Note 15)	Include	Exclude
S1	South East SA	Include	Exclude
S2	Riverland	Exclude	Include
S3	Mid-North SA	Include	Exclude
S4	Yorke Peninsula	Exclude	Exclude
S5	Northern SA	Exclude	Include
S6	Leigh Creek	Exclude	Exclude
S7	Roxby Downs	Exclude	Include
S8	Eastern Eyre Peninsula	Include	Exclude
S9	Western Eyre Peninsula	Exclude	Exclude
S10	South East SA Coast	Exclude	Exclude
T1	North East Tasmania	Include	Exclude
T2	North West Tasmania	Include	Exclude
T3	Central Highlands	Include	Exclude
T4	North Tasmania Coast	Exclude	Exclude

Figure 1 REZ by energy type. Left panel shows map of REZ coloured by energy type, and the table on the right shows which REZ are included in the Part-1 analysis for each energy type.

Definition of VRE lulls

VRE lulls occur when there is a reduction in solar and/or wind power generation. From a meteorological perspective, these can then be defined as a reduction in solar and/or wind resources below a specified threshold. Richardson et al. (2023) used a threshold to define lulls as the daily mean resource value being below the 25th percentile, where the percentile value is

calculated across all REZ. For this study, we employ a 5th percentile threshold applied to the 3-day running mean NEM-wide BARRA-C2 wind speed at 150m ($wind_{150}$) and Surface Downwelling Shortwave Radiation (rsds) and calculate over all available years since 2000 (2000-2023). Figure 2 shows the percentile distribution of REZ average mean 3-day $wind_{150}$ and 3-day rsds. The respective 5th percentile values are 5.17 m/s and 109.16 W/m^2. Days with NEM-wide 3-day mean resource values below the 5th percentile are deemed to be lull days. Noting that the frequency and duration of VRE lull events is highly dependent on the chosen threshold.

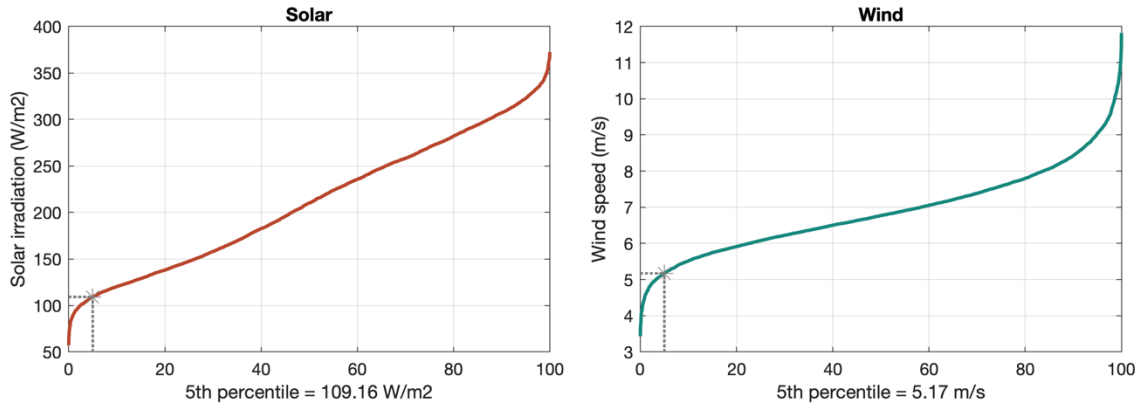

Figure 2 percentile distribution of the NEM-wide average 3-day running mean (left) solar irradiation (rsds) and (right) $wind_{150}$: the respective 5th percentile values used for defining lulls are 5.17m/s and 109.16 W/m^2. Days with NEM-wide 3-day mean resource values below the 5th percentile are deemed to be lull days.

Identification of VRE lulls

Lulls are defined as days when wind, solar, or combined resource values are below the 5th percentile. Figure 3 illustrates the identification of NEM-wide lulls in 2010.

NEM-wide average 3-day mean resource values ($wind_{150}$ in m/s and rsds in W/m^2) are converted to percentiles using the distributions shown in Figure 2. When the 3-day running mean resource value is below the 5th percentile value ($wind_{150}$ < 5.17m/s; rsds < 109.16 W/m^2), the percentile value will be below 5 and a lull will be declared.

To identify compound lulls, the 3-day running mean wind and solar percentile values are averaged to produce a compound lull index which is then re-normalised to percentiles; days when this index is below 5 are declared to be compound lull days. Using this approach, there are on average ~18 lull days per year for wind, solar, and compound lulls. Figure 4 shows an example of a wind, solar, and compound lull event identified in June-July 2010.

As a validation exercise, the approach is benchmarked against two multi-day VRE lulls experienced during May and June 2024. Figure 5 shows a comparison between observed NEM-wide power output and compound lulls identified from wind and solar resource availability. The percentile-based approach successfully identifies periods of low resource availability in May and June 2024, consistent with observations.

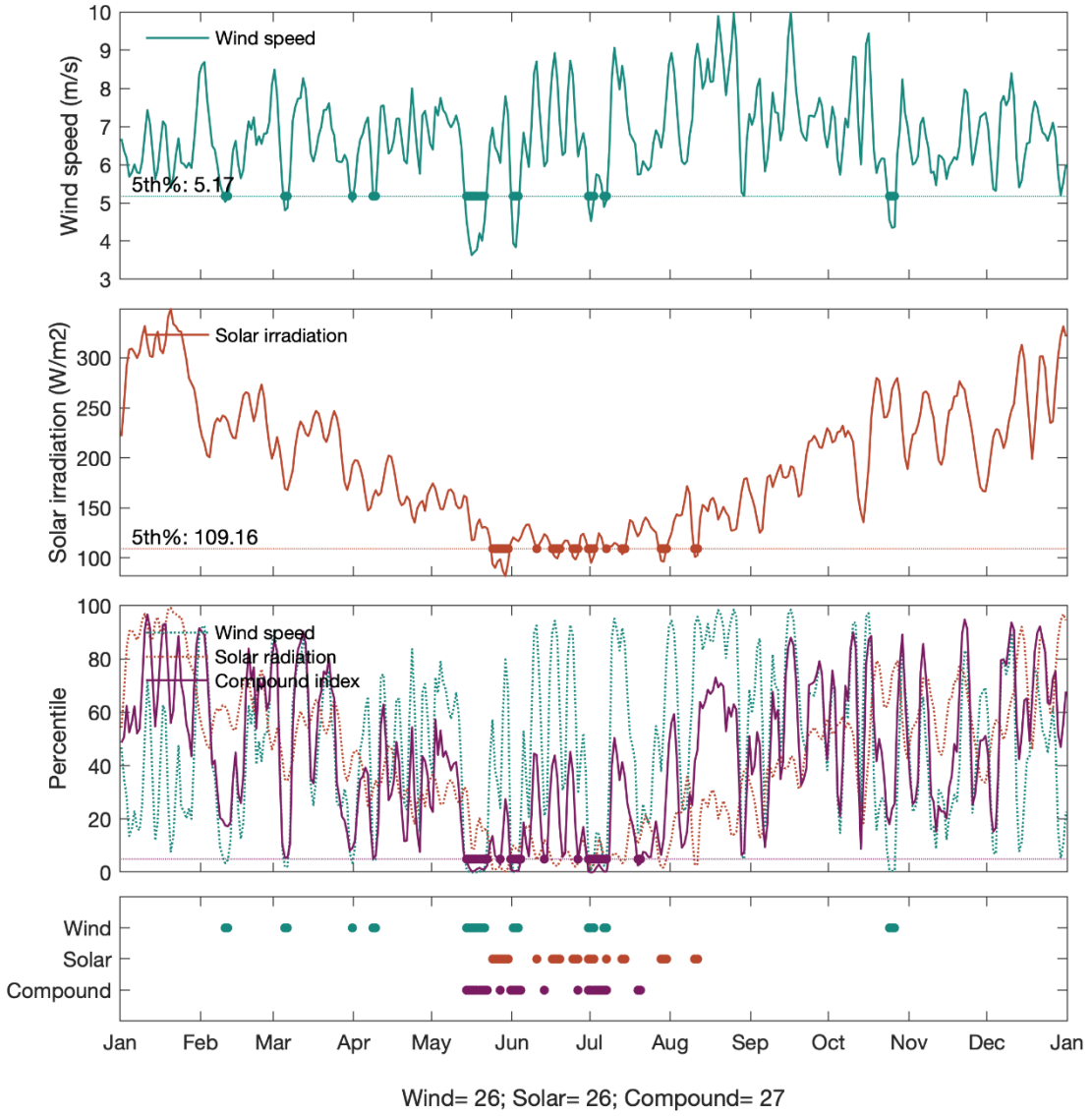

Figure 3 Example of NEM-wide VRE lull identification during 2010 for wind (upper panel), solar (2nd panel) and compound (3rd panel) events. All values are NEM-wide average 3-day running means. For wind and solar, solid lines are the actual resource value in m/s or W/m²; dotted lines in the 3rd panel are the same values converted to percentiles; dashed lines represent the 5th percentile threshold, days with resource values below the 5th percentile are indicated by solid dots. In the 3rd panel, all values are percentiles. The lower panel shows a summary of identified lull days for wind, solar, and compound events.

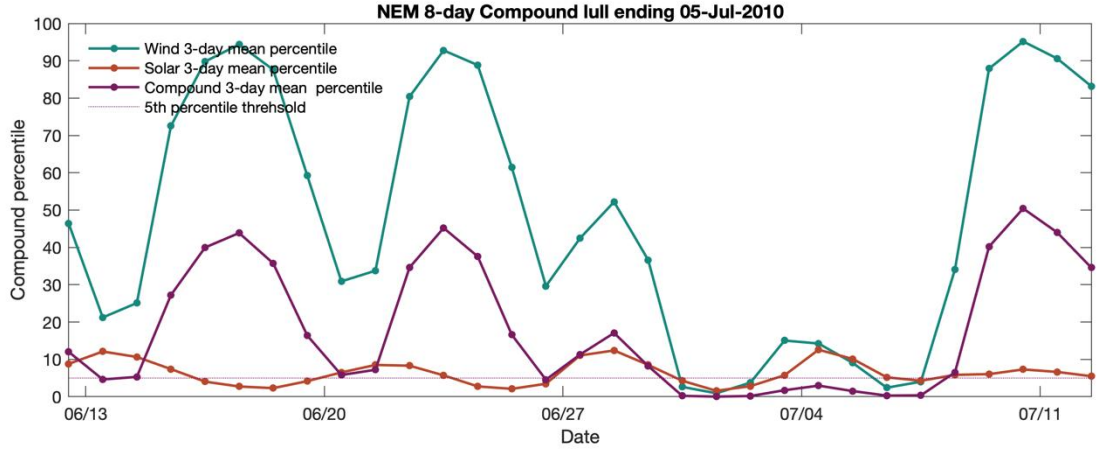

Figure 4 Example of a wind, solar, and compound VRE lull event identified during 2010. Lulls are days when the NEM-wide average 3-day running mean resource value is below the 5th percentile. In this figure, daily wind and solar values have been converted to percentiles for comparison, and to allow them to be averaged into a compound lull index. The compound lull index has been re-normalised to identify days when it is below its 5th percentile value.

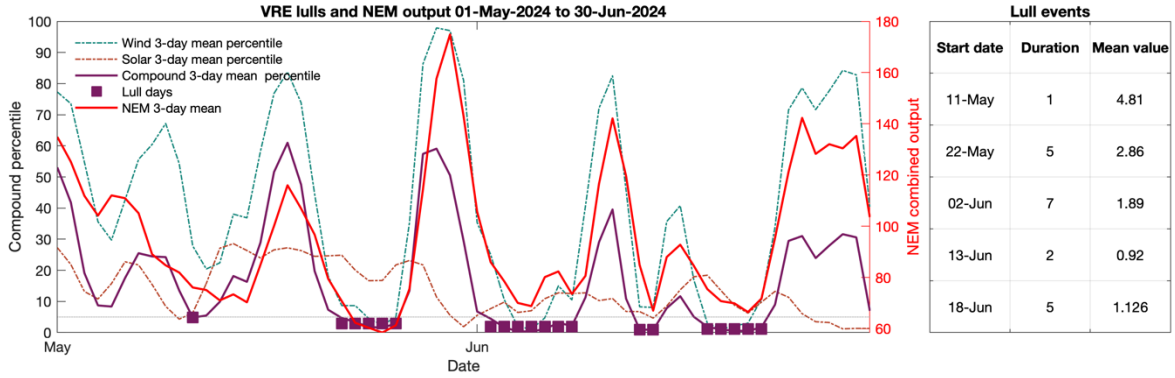

Figure 5 NEM-wide output (red) during observed VRE lull events is used to benchmark the lull identification approach. In 2024, the NEM experienced two severe multi-day lull events during May and June. The percentile-based approach identified these events as periods of low resource availability. The red line indicates NEM-wide 3-day mean output in GWh; the solid purple line represents the normalised compound lull index. Estimation of GWh is described in detail in Part 2 and involves calibrating historical daily weather data to daily average wind and solar traces, then multiplying by REZ capacity to estimate daily output in GWh.

Frequency and duration of VRE lulls

The percentile-based approach to VRE lull identification, when using the 5th percentile threshold, produces an average of ~18 lulls per year over the 2000-2023 period. Lull frequency during individual years will be higher or lower than average due to weather variability.

Figure 6a shows the annual number of NEM-wide lull days for wind, solar and compound lulls over the 1980-2023 period. Since 1980 there has been a clear decreasing trend in the frequency of solar lulls, no clear trend in wind lull frequency, and a small decreasing trend in compound lull frequency.

Solar lulls show a clear season cycle that aligns with the solar cycle (Figure 6b); lull days are rare between September to March (Spring equinox to Autumn equinox) and are more likely between April and August, with peak frequency in June (Winter solstice). Wind lulls have a more subdued seasonal cycle compared to solar lulls; they can occur at any time of year but tend to be less frequent during Winter and Spring, and more frequent during Summer and Autumn, with peak

frequency during May. The seasonal cycle for compound lulls corresponds closely to solar lulls with peak activity in May, June, and July.

Figure 6c shows that solar lulls tend to have the longest durations, up to a maximum duration of 20 days, while wind lulls have shorter durations, with the longest observed event lasting 8 days. Compound lulls typically last for 1-3 days, with the longest event lasting 16 days.

When only NSW REZ are included in the analysis, there is an increase in the frequency and duration of all lull types (Figure 7). This is because the entire NEM spans a diverse geographic range and individual REZs tend to experience lulls at different times. For example, solar lulls are less frequent in more northern Queensland REZs, while wind lulls are less frequent in more southern Victorian and Tasmanian REZs (Figure 8). When fewer REZs are included in the energy mix, the frequency and duration of lulls increase.

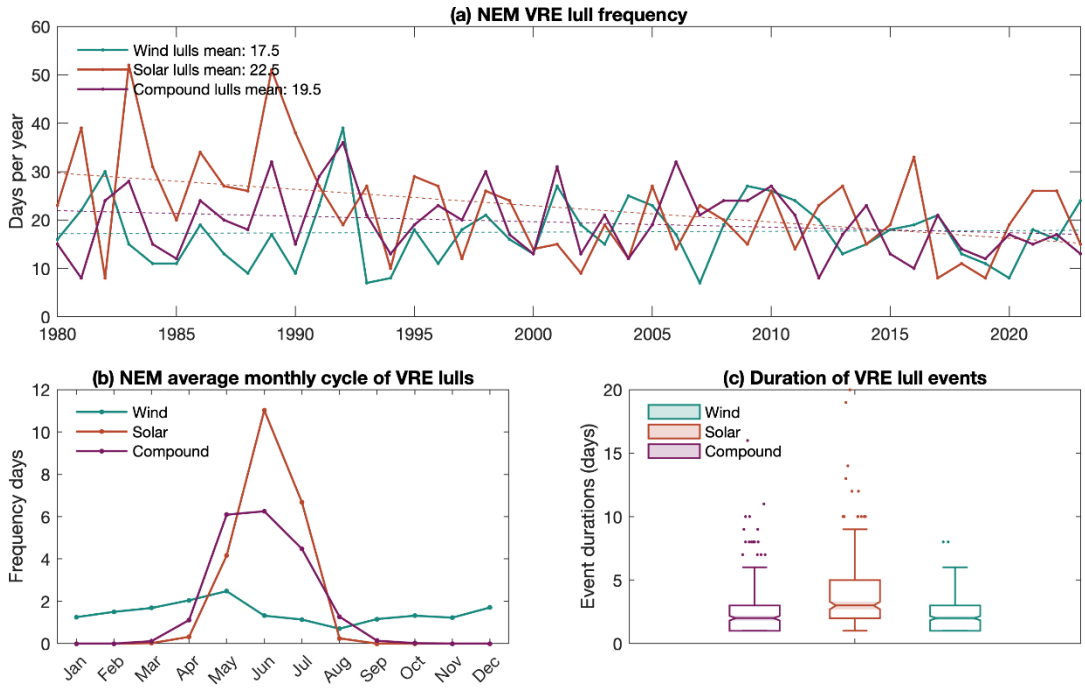

Figure 6 (a) Annual frequency of NEM-wide VRE lull days for wind, solar, and compound lulls. (b) Average frequency of lull days per month over the 1980-2023 period. (c) Boxplots showing the duration in days of all lull events over the 1980-2023 period

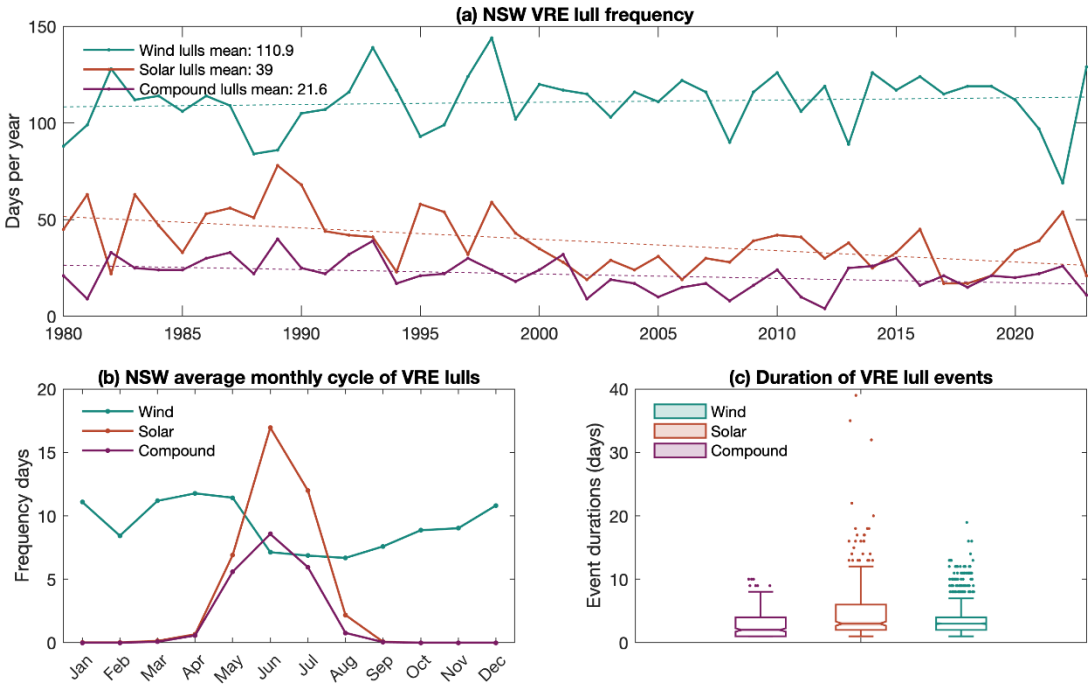

Figure 7 As for Figure 6 above but including NSW only REZs while using the same thresholds as the NEM-wide analysis

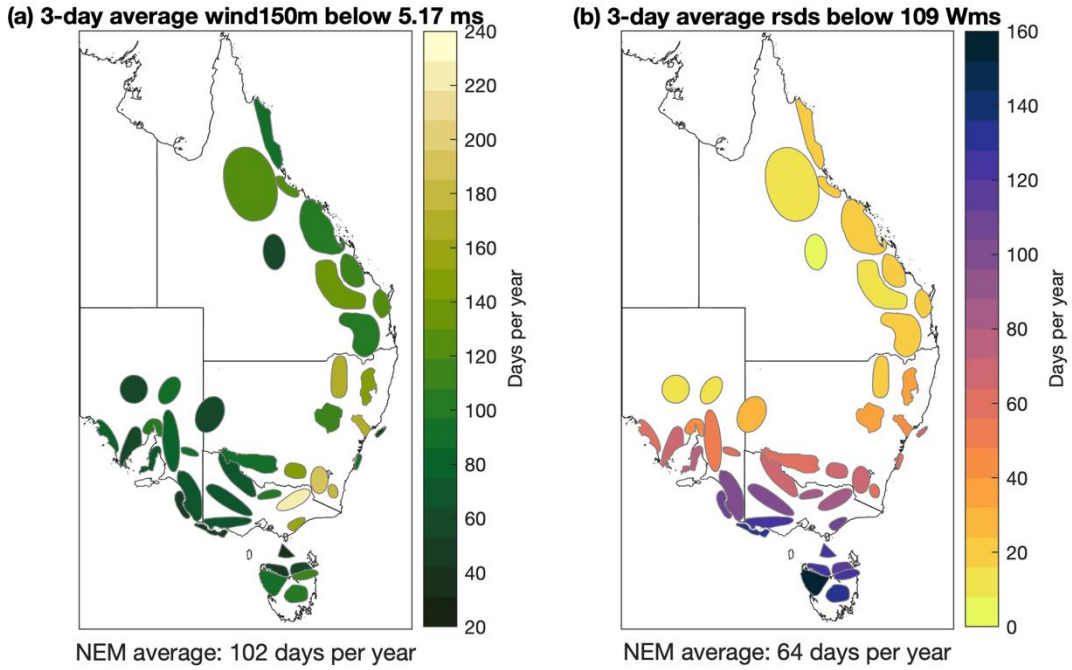

Figure 8 Annual average frequency of VRE lulls days at each REZ for (a) days with 3-day average wind$_{150}$ below 5.17m/s, and (b) days with 3-day average solar irradiation (rsds) below 109 Wm^2.

Possible future changes in VRE lulls from RCM

Possible future changes in the frequency and duration of VRE lulls are examined using the BARPA ensemble of RCM simulations under two plausible scenarios: SSP126 and SSP370 (see Appendix 2 for details on scenarios and climate model datasets). Lulls are identified from bias corrected daily

model data, using the same approach as for historical data; lulls are defined as days when the NEM-wide 3-day mean $wind_{150}$, rsds, or compound lull index are below the 5th percentile, where percentiles are calculated relative to the 2000-2023 period.

VRE lull frequency

Projections shown for wind lulls (Figure 9), solar lulls (Figure 10), and compound lulls (Figure 11), are based on the 7-member ensemble mean 20-year averages. To focus on possible changes due to global warming, it is necessary to calculate 20-year averages to "smooth-out" natural variability, such as year-to-year variations caused by the El Nino Southern Oscillation (ENSO). It is then possible to average across different models to calculate a multi-model ensemble mean. Individual events from future climate simulations are examined in more detail in Part 2.

The difference between models, shown as 1-standard deviation shading in Figure 9, 10, and 11, represents uncertainty in projections due to the way different models simulate future climate. This is one measure of uncertainty in the projections: where there is agreement (disagreement) between models, there tends to be higher (lower) confidence in projections.

Projections for wind lull frequency show a small increasing trend under both SSP126 and SSP370 scenarios. This trend is consistent with the observational record which also shows a slight increasing trend since 1990. Figure 9 suggests that this increase will mostly occur during late Autumn (April and May), and late Winter (August).

Projections for solar lulls show a decreasing trend for SSP126 and SSP370, with lulls becoming less frequent further into the future and under the higher emission SSP370 scenario (Figure 10). This trend is consistent with the observed decrease in solar lull frequency since 1990. Figure 10 suggests the decrease will occur mostly during June and July when solar lulls are currently most frequent.

Projections for compound lulls show no trend under SSP126 or SSP370 scenarios (Figure 11).

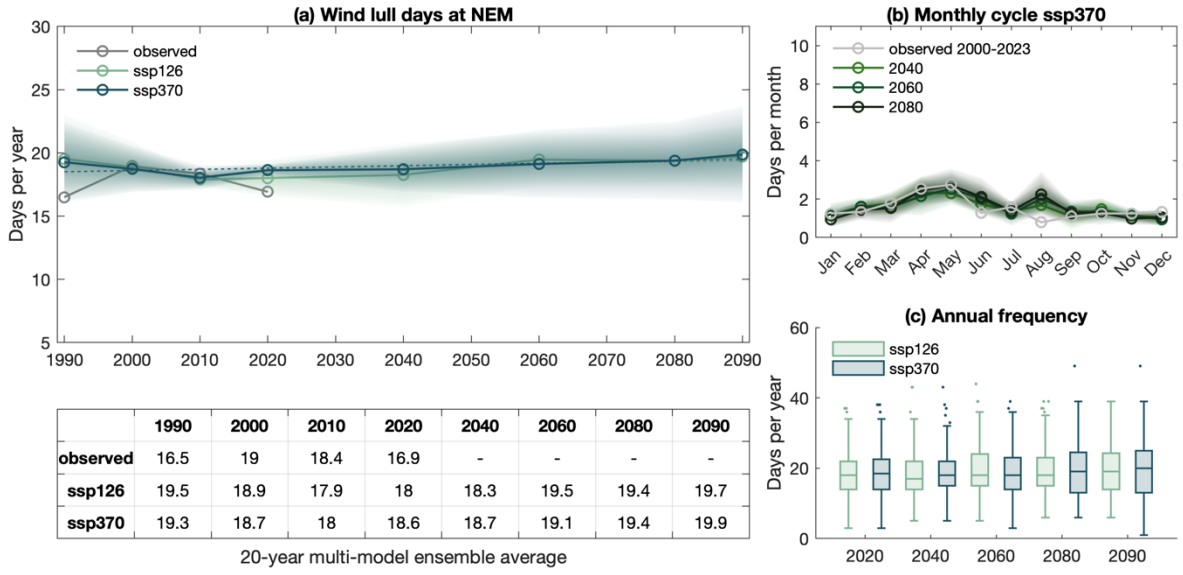

	1990	2000	2010	2020	2040	2060	2080	2090
observed	16.5	19	18.4	16.9	-	-	-	-
ssp126	19.5	18.9	17.9	18	18.3	19.5	19.4	19.7
ssp370	19.3	18.7	18	18.6	18.7	19.1	19.4	19.9

Figure 9 Frequency of wind lulls from observations since 1990 and RCM projections for SSP126 and SSP370 scenarios. (a) annual frequency of lull days, solid lines are the 20-year average multi-model ensemble mean, where shading shows 1-standard deviation of the ensemble mean and represents differences between different models. 20-year averaging highlights possible changes due to global warming but hides year-to-year variability. Values in the table correspond to 20-

year averages in (a). (b) shows the average monthly cycle of wind lulls, future time periods are the 20-year average centred on each year, where 2040 is the average of 2031-2050; shading represent 1-standard deviation of the multi-model ensemble mean. (c) boxplots showing annual number of lull days during each 20-year period from all model simulations under SSP126 and SSP370 scenarios.

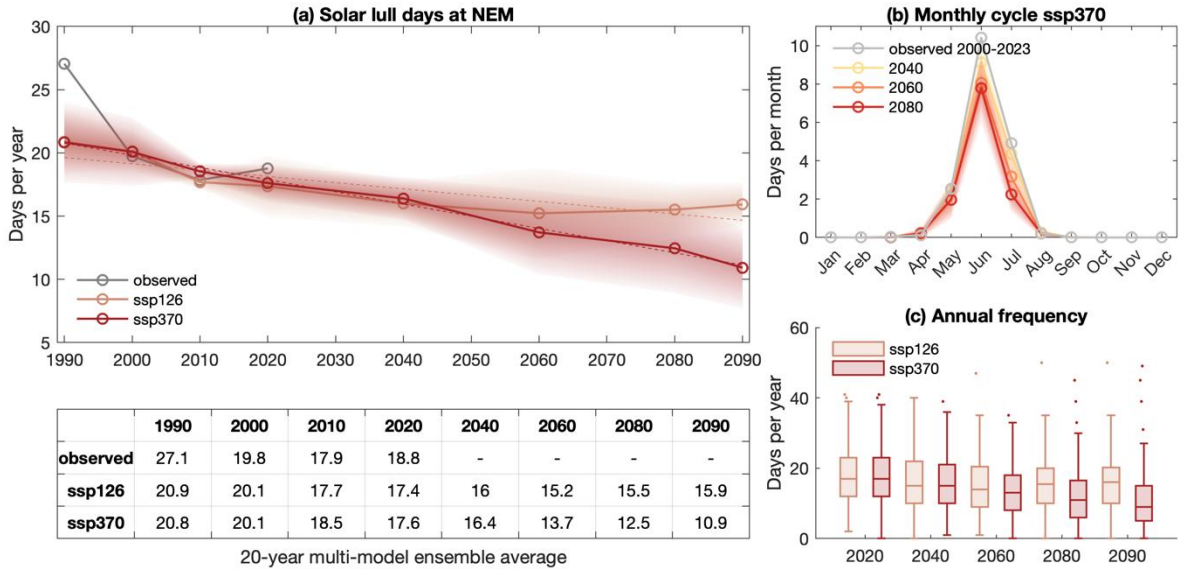

	1990	2000	2010	2020	2040	2060	2080	2090
observed	27.1	19.8	17.9	18.8	-	-	-	-
ssp126	20.9	20.1	17.7	17.4	16	15.2	15.5	15.9
ssp370	20.8	20.1	18.5	17.6	16.4	13.7	12.5	10.9

20-year multi-model ensemble average

Figure 10 Frequency of solar lulls from observations since 1990 and regional climate model projections for SSP126 and SSP370 scenarios. (a) annual frequency of lull days, solid lines are the 20-year average multi-model ensemble mean, where shading shows 1-standard deviation of the ensemble mean and represents differences between different models. 20-year averaging highlights possible changes due to global warming but hides year-to-year variability. Values in the table correspond to 20-year averages in (a). (b) shows the average monthly cycle of solar lulls, future time periods are the 20-year average centred on each year, where 2040 is the average of 2031-2050; shading represent 1-standard deviation of the multi-model ensemble mean. (c) boxplots showing annual number of lull days during each 20-year period from all model simulations under SSP126 and SSP370 scenarios.

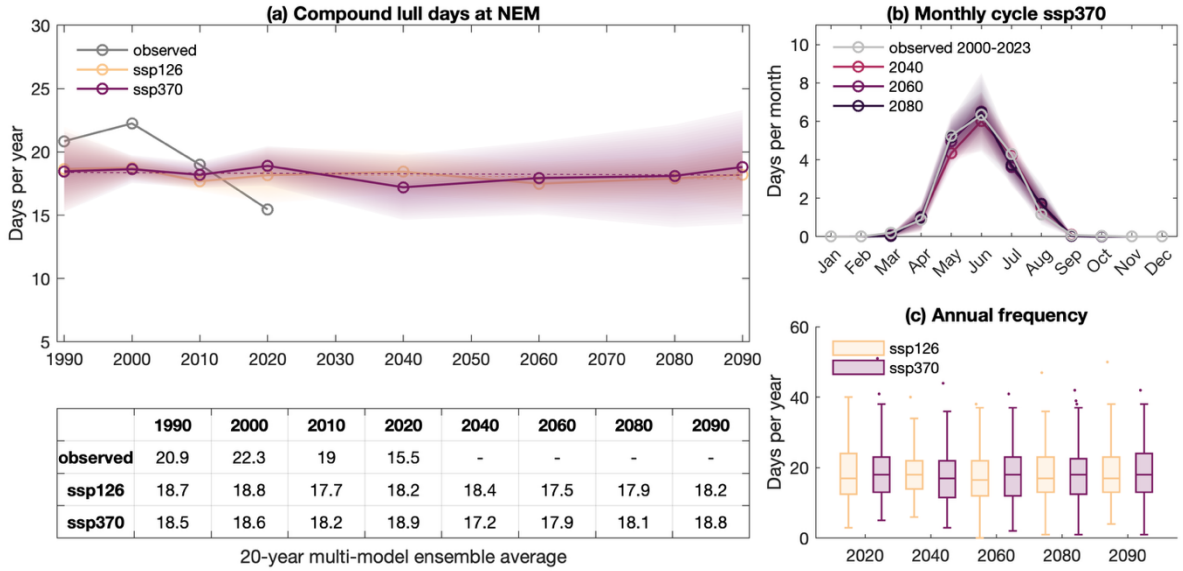

	1990	2000	2010	2020	2040	2060	2080	2090
observed	20.9	22.3	19	15.5	-	-	-	-
ssp126	18.7	18.8	17.7	18.2	18.4	17.5	17.9	18.2
ssp370	18.5	18.6	18.2	18.9	17.2	17.9	18.1	18.8

20-year multi-model ensemble average

Figure 11 Frequency of compound lulls from observations since 1990 and regional climate model projections for SSP126 and SSP370 scenario. (a) annual frequency of lull days, solid lines are the 20-year average multi-model ensemble mean, where shading shows 1-standard deviation of the ensemble mean and represents differences between different models. 20-year averaging highlights possible changes due to global warming but hides year-to-year variability. Values in the table correspond to 20-year averages in (a). (b) shows the average monthly cycle of compound lulls, future time periods are the 20-year average centred on each year, where 2040 is the average of 2031-2050; shading represent 1-standard deviation of

the multi-model ensemble mean. (c) boxplots showing annual number of lull days during each 20-year period from all model simulations under SSP126 and SSP370 scenarios.

VRE lull durations

VRE lull durations are measured as the number of consecutive days when wind, solar, or compound wind and solar resources are below the 5th percentile. Figure 12, 13, and 14 show the duration of VRE lull events from observation-based data (BARRA-C2) over the 1990 to 2023 period, and from the BARPA ensemble for 1990 to 2099 under SSP126 and SSP370 scenarios.

Wind lull events currently last on average ~2 days (Figure 12a), with some individual events lasting up to 10 days (Figure 12c). There is no strong seasonal cycle; however, events do appear to be slightly longer during May and shorter during November and December. Under future climate scenarios, the BARPA ensemble shows no significant change in the duration of wind lull events under either scenario.

Solar lull events currently last on average 3.7 days (Figure 13a), with some individual events lasting up to 20 days (Figure 13c). There is a strong seasonal cycle with most events occurring between March and August, and peak duration in June. Under future climate scenarios the BARPA ensemble shows a decreasing trend in the duration of solar lull events where the trend is stronger under SSP370 compared to SSP126.

Compound lull events currently last on average 2-3 days (Figure 14a), with some individual events lasting over 15 days (Figure 14c). There is a strong seasonal cycle similar to solar lulls, with most events occurring between March and August, and peak durations in May, June, and July. Under future climate scenarios, the BARPA ensemble shows no clear trend in the duration of compound lull events under either scenario.

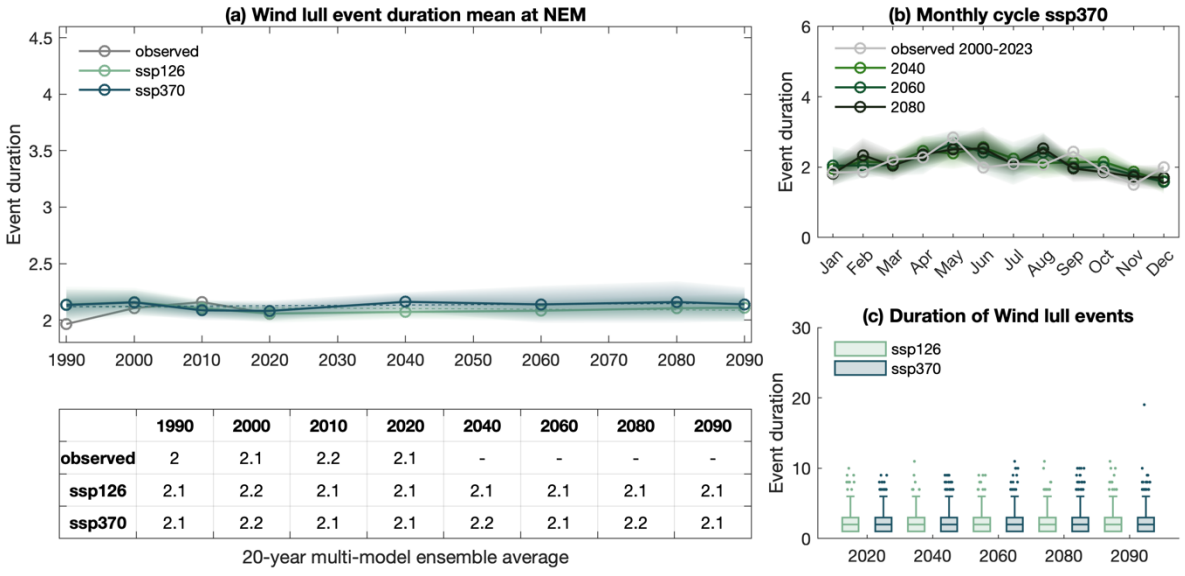

	1990	2000	2010	2020	2040	2060	2080	2090
observed	2	2.1	2.2	2.1	-	-	-	-
ssp126	2.1	2.2	2.1	2.1	2.1	2.1	2.1	2.1
ssp370	2.1	2.2	2.1	2.1	2.2	2.1	2.2	2.1

Figure 12 Average duration of wind lull events from observations since 1990 and regional climate model projections for SSP126 and SSP370 scenarios. (a) average duration of lull events, solid lines are the 20-year average multi-model ensemble mean, where shading shows 1-standard deviation of the ensemble mean and represents differences between different models. 20-year averaging highlights possible changes due to global warming but hides year-to-year variability. Values in the table correspond to 20-year averages in (a). (b) shows the average monthly cycle of wind lull event durations, future time periods are the 20-year average centred on each year, where 2040 is the average of 2031-2050; shading represent 1-standard deviation of the multi-model ensemble mean. (c) boxplots showing duration of all lull events during each 20-year period from all model simulations under SSP126 and SSP370 scenarios.

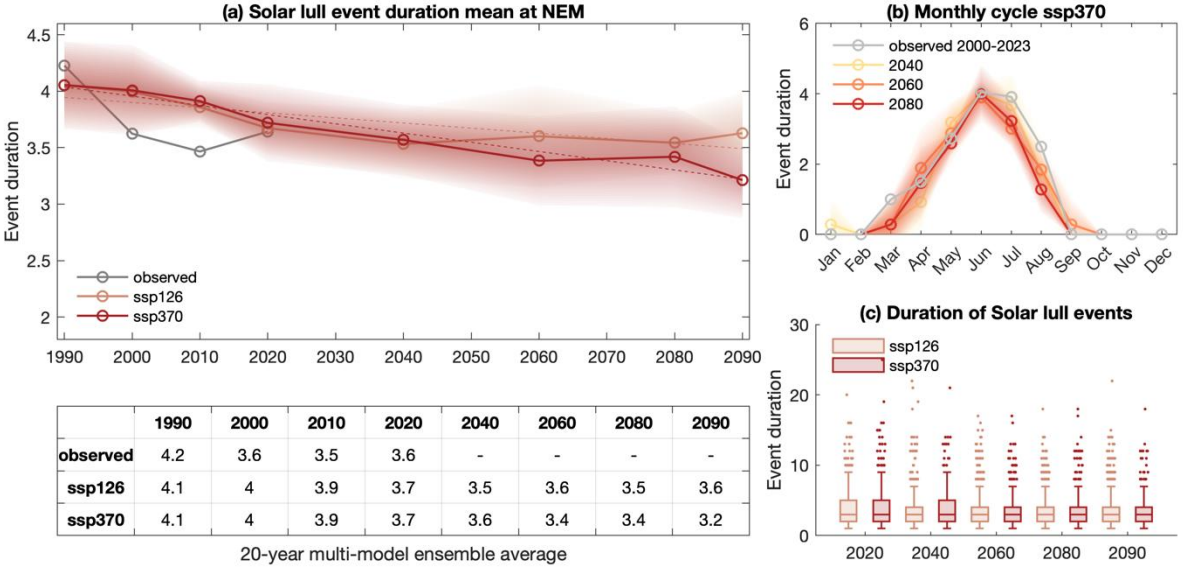

	1990	2000	2010	2020	2040	2060	2080	2090
observed	4.2	3.6	3.5	3.6	-	-	-	-
ssp126	4.1	4	3.9	3.7	3.5	3.6	3.5	3.6
ssp370	4.1	4	3.9	3.7	3.6	3.4	3.4	3.2

20-year multi-model ensemble average

Figure 13 Average duration of solar lull events from observations since 1990 and regional climate model projections for SSP126 and SSP370 scenarios. (a) average duration of lull events, solid lines are the 20-year average multi-model ensemble mean, where shading shows 1-standard deviation of the ensemble mean and represents differences between different models. 20-year averaging highlights possible changes due to global warming but hides year-to-year variability. Values in the table correspond to 20-year averages in (a). (b) shows the average monthly cycle of solar lull event durations, future time periods are the 20-year average centred on each year, where 2040 is the average of 2031-2050; shading represent 1-standard deviation of the multi-model ensemble mean. (c) boxplots showing duration of all lull events during each 20-year period from all model simulations under SSP126 and SSP370 scenarios.

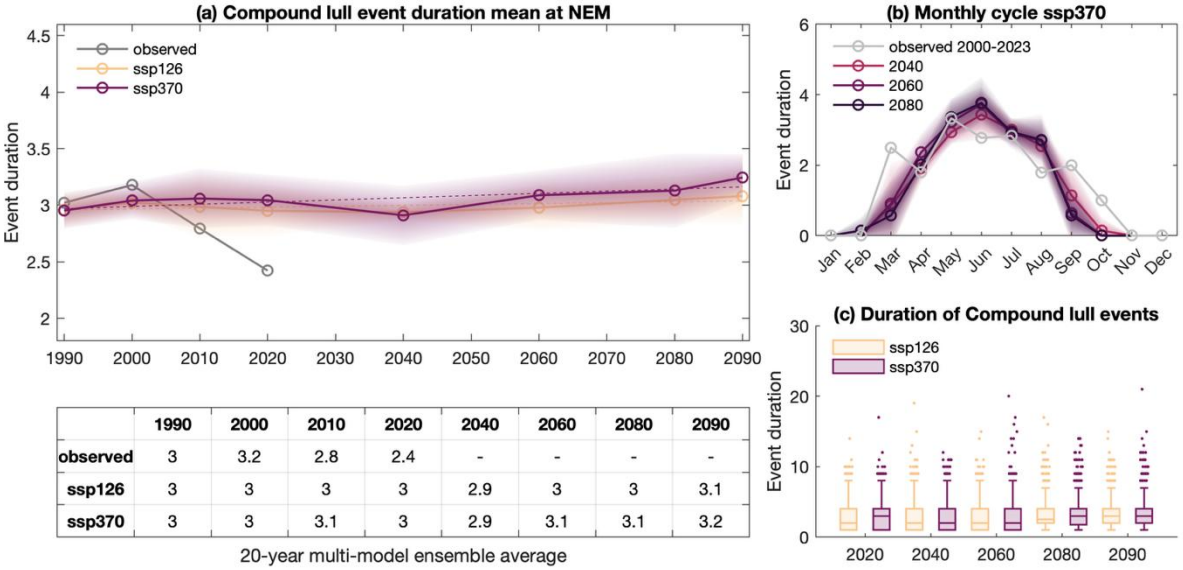

	1990	2000	2010	2020	2040	2060	2080	2090
observed	3	3.2	2.8	2.4	-	-	-	-
ssp126	3	3	3	3	2.9	3	3	3.1
ssp370	3	3	3.1	3	2.9	3.1	3.1	3.2

20-year multi-model ensemble average

Figure 14 Average duration of compound lull events from observations since 1990 and regional climate model projections for SSP126 and SSP370 scenarios. (a) average duration of lull events, solid lines are the 20-year average multi-model ensemble mean, where shading shows 1-standard deviation of the ensemble mean and represents differences between different models. 20-year averaging highlights possible changes due to global warming but hides year-to-year variability. Values in the table correspond to 20-year averages in (a). (b) shows the average monthly cycle of compound lull event durations, future time periods are the 20-year average centred on each year, where 2040 is the average of 2031-2050; shading represent 1-standard deviation of the multi-model ensemble mean. (c) boxplots showing duration of all lull events during each 20-year period from all model simulations under SSP126 and SSP370 scenarios.

Temperature during lull events

Daily maximum and overnight minimum temperatures during compound lull events are examined for historical observations and future climate scenarios. Compound lulls occur primarily during the coldest months of the year (May, June, and July), when solar irradiance is at a minimum. When averaged across all of NSW, maximum (daytime) temperatures are lower during compound lull days compared with non-lull days, while minimum (overnight) temperatures are higher during compound lull days compared with non-lull days (Figure 15).

BARPA RCM projections show that, under a warming climate, daily maximum and minimum temperatures will increase, with higher increases further into the future (Figure 15). Maximum (minimum) temperatures will continue to be lower (higher) during compound lull days compared with non-lull days.

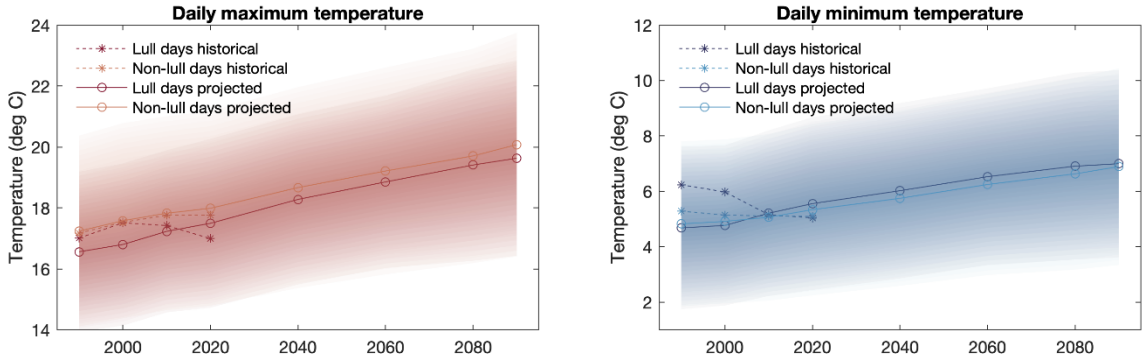

Figure 15 Average daily (a) maximum and (b) minimum temperature during lull days, compared to non-lull days over the historical period from 1981-2023 and BARPA regional climate model projections under the combined SSP126 and SSP370 scenarios. Analysis is restricted to May-June-July as being the months most affected by VRE lulls. Projections display an increasing trend in temperatures, with non-lull days on average warmer (cooler) than lull days for maximum (minimum) temperatures. Shading is indicative of daily temperature variability and represents 1-standard deviation of daily values from the multi-model 20-year sample for each time period, where for example 2040 is represented by daily temperatures between 2031 and 2050 from all models and scenarios.

Rainfall and drought projections

Water security and drought can potentially pose a risk to hydroelectric power generation. Water security refers to the availability of water for socioeconomical requirements, while the term drought is commonly used to describe water deficits. This section examines hydroclimate projections in terms of total annual rainfall and soil moisture index (SMI) across the NEM, with a focus on the locations of hydroelectric dams.

Total annual rainfall provides an indicator of water availability, while the SMI provides an indicator of drought in terms of moisture in the landscape. The SMI represents soil moisture relative to the 5th and 95th percentile, normalised and scaled from 5.0 to −5.0, with 5.0 representing soil moisture at field capacity and −5.0 representing soil moisture at wilting point (Hunt, 2009). Regions with lower average SMI values are more prone to drought.

BARPA regional climate model simulations provide an indication of future trends in overall water availability and drought conditions. Projections for total annual rainfall (Figure 16) indicate a general decrease over most of the NEM, except for parts of northern and eastern Australia. Projections for SMI show a spatial pattern similar to total rainfall projections (Figure 17), with

increasing soil moisture over parts of northern and eastern Australia and decreasing soil moisture in the southeast. BARPA RCM simulations show that most of the 30-largest hydroelectric dam locations across the NEM will experience decreasing rainfall and soil moisture by 2050 and 2090 (Figure 18 and Figure 19).

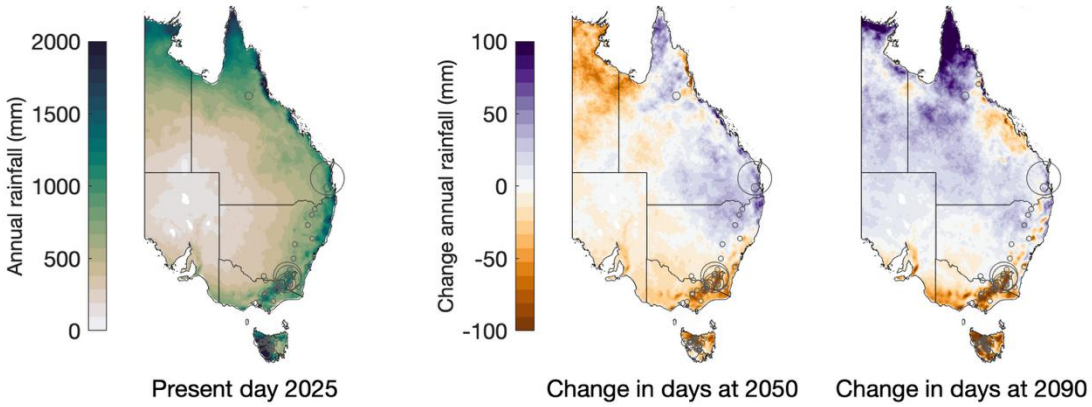

Figure 16 Simulation of total annual rainfall from the BARPA ensemble for present day and change at future time periods (2050 and 2090) under the SSP370 scenario. Values are the multi-model ensemble mean 20-year average centred on the displayed year, where 2050 is the average of 2041 to 2060. Hydroelectric dams are shown as circles, where the circle size is scaled relative to dam capacity.

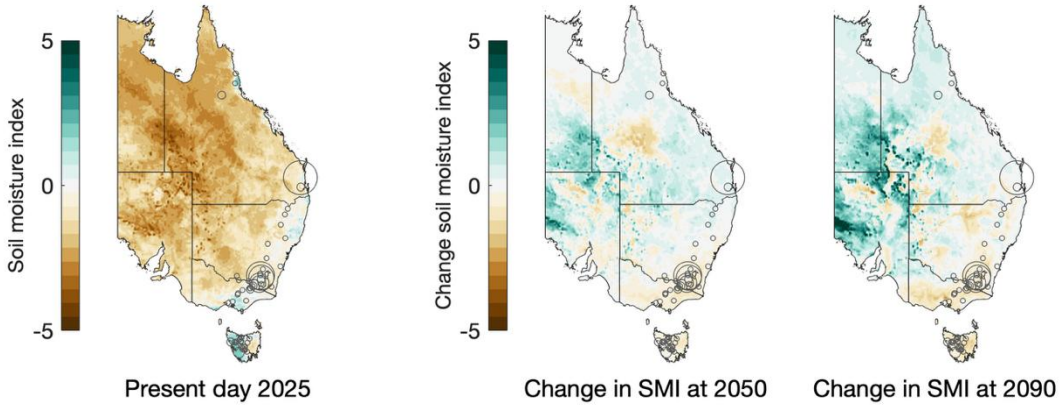

Figure 17 Simulation of annual average soil moisture index (SMI) from the BARPA ensemble for present day and change at future time periods (2050 and 2090) under the SSP370 scenario. The SMI represents modelled soil moisture on a scale of -5 to 5, where -5 represent soil moisture at or below the 5th percentile while 5 is at or above 95th percentile. Values are the multi-model ensemble mean 20-year average centred on the displayed year, where 2050 is the average of 2041 to 2060. Hydroelectric dams are shown as circles, where the circle size is scaled relative to dam capacity.

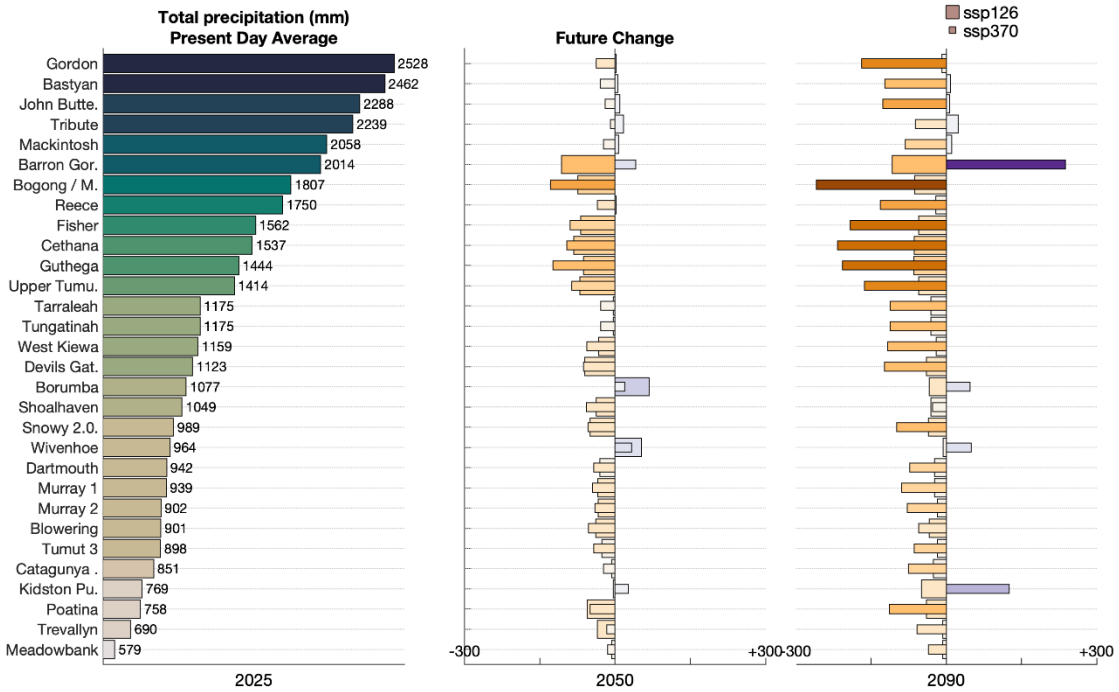

Figure 18 RCM simulations of total annual rainfall at the 30 largest dams in the NEM from the BARPA ensemble for present day and change at future time periods (2050 and 2090) under the SSP126 and SSP370 scenarios. Values are the multi-model ensemble mean 20-year average centred on the displayed year, where 2050 is the average of 2041 to 2060.

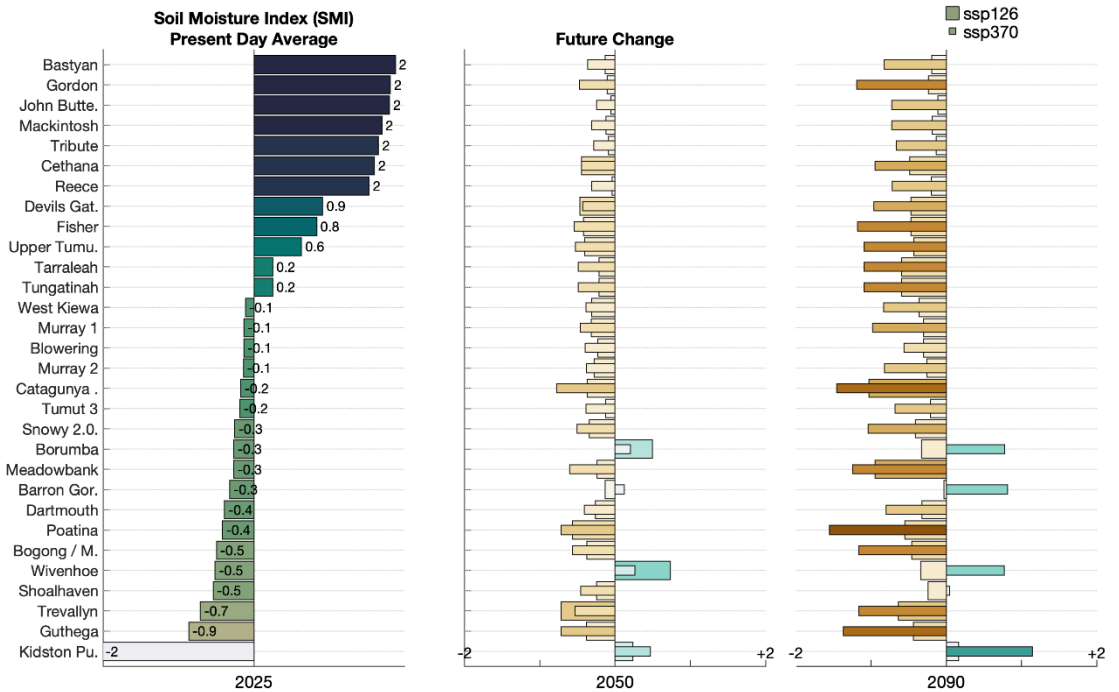

Figure 19 RCM simulations for annual average SMI at the 30 largest dams in the NEM from the BARPA ensemble for present day and change at future time periods (2050 and 2090) under the SSP126 and SSP370 scenarios. Values are the multi-model ensemble mean 20-year average centred on the displayed year, where 2050 is the average of 2041 to 2060.

Climate system influence on VRE lulls

Individual VRE lulls occur due to synoptic scale weather events. This section investigates the synoptic weather patterns associated with lull days, and seasonal relationship with the three main climate drivers known to influence weather and climate across the NEM: El Niño-Southern Oscillation (ENSO), the Indian Ocean Dipole (IOD) and the Southern Annular Mode (SAM).

Climate driver relationships

The major climate drivers (ENSO, IOD, and SAM) have a strong influence on the Australian climate, including cloudiness and wind. However, due to large spatial variability in teleconnections, different regions will often experience different responses. Richardson et al. (2023) found the NEM to be largely resilient to climate driver influences because it spans such a large geographic range.

General relationships with the three main climate drivers are summarised in Figure 20 where boxplots show the number of lull days occurring during positive, neutral, and negative phases of the Southern Oscillation Index (SOI; representing ENSO), the Dipole Mode Index (DMI; representing the IOD), and the SAM index. Analysis is restricted to the May-June-July season when NEM-wide solar and compound lulls are most frequent. Positive and negative phases are seasons where the climate index values are greater than +/- 1 standard deviation from the mean. Neutral phases are seasons when the index values are between -1 and +1 standard deviation from the mean.

Wind lulls show no clear relationships with any of the main climate drivers during May-June-July but may be more frequent during neutral phases of SOI and IOD. Solar lulls are more frequent during La Niña (average of 31 days per season) compared to neutral or El Niño (average of 17 days). Solar lulls are also more frequent during DMI negative (average of 28 days) and slightly more frequent during SAM positive (average of 26 days). NEM-wide compound lulls do not appear to be strongly influenced by the three main climate drivers but may be slightly more common during La Nina and SAM positive.

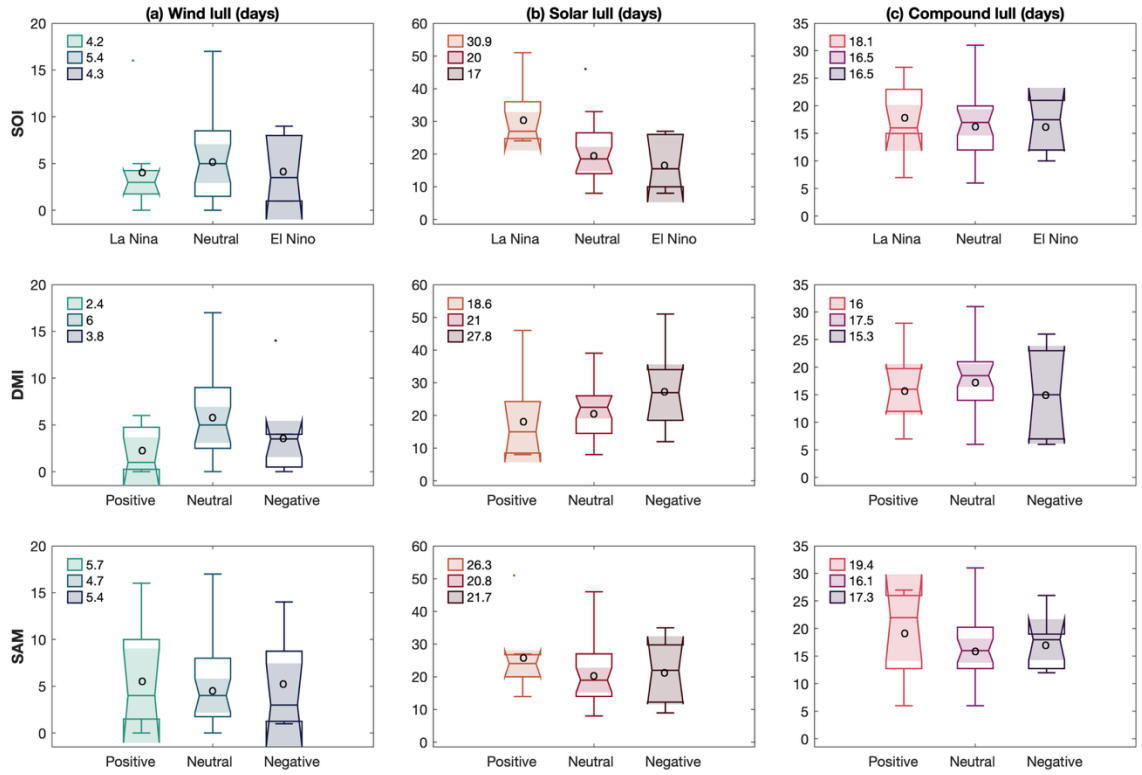

Figure 20 The number of lull days (wind, solar and compound) during positive, neutral and negative phases of the three main climate drivers known to influence seasonal climate across the NEM. Numbers in the figure legends show the average number of lull days for all positive, neutral, and negative phases. Analysis is restricted to the May-June-July period when NEM-wide compound lulls are most common.

Synoptic weather associated with VRE lulls

Understanding the synoptic weather patterns during VRE lulls days can help to explain the cause of lull events, and the likely weather during events which may influence demand. Figure 21 shows average daily anomalies (difference from the long-term monthly average) of maximum air temperature, cloud cover, and atmospheric circulation (mean sea level pressure and winds) for all wind, solar, and compound lull days identified between 2000 to 2023. The analysis is restricted to the May-June-July period when compound lulls are most frequent.

Wind lulls tend to occur when the main region of high pressure is to the south of the Australian continent, and there is a weakening or reversal of the dominant westerly airflow over southeast. This situation can occur during Blocking High events. There also tends to be increased cloud cover over the eastern seaboard.

Solar lulls are associated with low atmospheric pressure over southeast Australia and cyclonic (clockwise) wind circulation typical of low-pressure systems. This situation can occur during general low-pressure systems, and can be more persistent during Cut-off Low events. During solar lulls, daytime maximum temperatures are lower than average over much of inland NSW and Queensland, and cloud cover is increased over most of the NEM.

Compound lulls are associated with lower atmospheric pressure over central Queensland, together with higher pressure to the south of the continent and anomalous easterly airflow over Victoria. This situation can occur during Cut-off low or Northwest cloudband events, especially if they occur in conjunction with a Blocking High to the south. During compound lulls, daytime

maximum temperatures are lower than average over most of NSW and cloud cover is increased over most of the NEM.

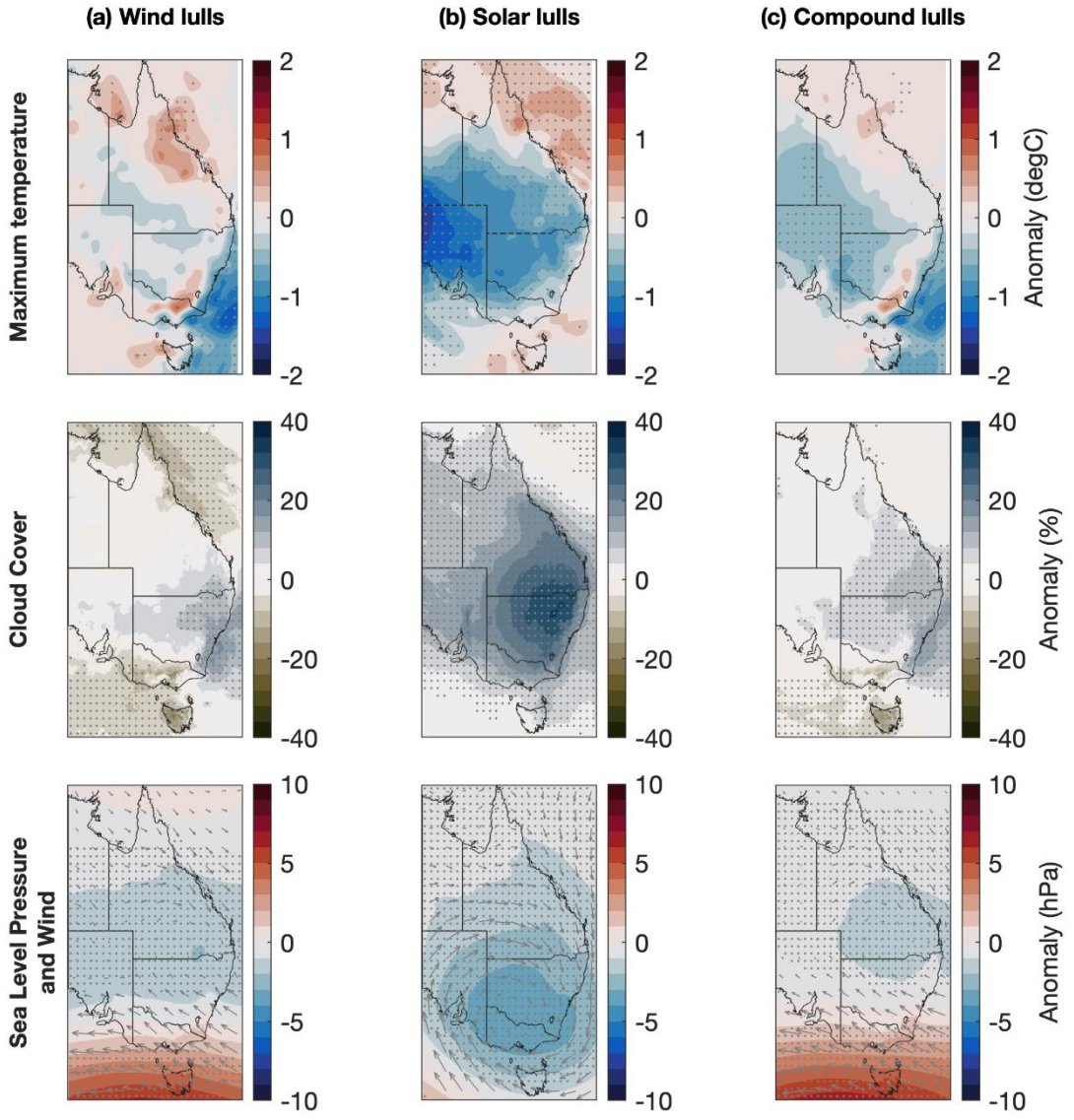

Figure 21 Synoptic composites of daily weather anomalies during (a) wind, (b) solar, and (c) compound lull events for daily maximum temperature, cloud cover and atmospheric circulation represented by sea level pressure and $Wind_{150}$. Composites are the average of daily anomalies for all events occurring in May, June, and July between 2000 and 2023. Daily anomalies are calculated relative to the 2000-2023 monthly mean. Stippling denotes regions where the VRE lull composite is statistically (t-test: p<0.01) different from the mean.

Discussion – bottom-up approach

The bottom-up approach investigates resource availability in terms of $wind_{150}$ and solar irradiation (rsds) across the NEM at key REZs shown in Figure 1, with the objective to identify the frequency and duration of VRE lulls under historical (observed) and possible future climate scenarios.

For this analysis, a lull is defined as a day when NEM-wide resource availability ($wind_{150}$, rsds, or combined) is below the 5th percentile relative to the 2000 to 2023 period – this definition results in 18.25 wind, solar lull and compound days per year over the 2000 to 2023 period. The approach

used here is intentionally stricter than that used by Richardson et al. (2023), with the objective of identifying only the most severe, NEM-wide lull events. Threshold choice and VRE lull definition strongly influences the frequency and duration of events but has minimal effect on the direction and magnitude of historical and future trends.

Observed VRE lull frequency, duration, and trends

Since 1980 there has been a decreasing trend in the frequency of solar lulls, a small increasing trend in the frequency of wind lulls, and no trend in compound lulls. There is a strong seasonal cycle to solar and compound lulls, with almost all events occurring in the months of lowest solar irradiation: May, June, and July. Wind lulls can occur at any time of year but tend to be more frequent in the Autumn months of April and May. Solar lulls have the longest durations lasting on average 3-4 days, with some individual events lasting longer than 15 days. Wind and compound lulls tend to be shorter, around 2-3 days with the longest events lasting around 10 days.

Future trends in VRE lulls

BARPA RCM simulations indicate that, under future warming scenarios, the frequency and duration of wind lulls will remain relatively consistent with historical observations. Solar lulls are expected to decrease in frequency and duration, and decreases will be larger under the higher emission SSP370 scenario. Compound lull frequency and duration is expected to remain relatively consistent with historical observations.

Observed and projected trends in solar lulls are consistent with the observed strengthening of atmospheric pressure over Australian continent, which is expected to continue with global warming (CSIRO, 2024). The Australian continent is typically dominated by large high-pressure systems. The expectation under a warming climate is that these high-pressure systems will strengthen and/or become more persistent. When this happens, cloud producing weather systems, including cold fronts, are pushed to the south and most of the continent experiences clear skies.

Temperatures during lull events

Compound and solar lulls occur during the coldest months of the year, when solar irradiation is at a minimum. Daytime maximum temperature across NSW is lower during compound lull events compared to non-lull events, while overnight minimum temperatures are higher. During compound lull events there is an increase in cloud cover. Increased cloud cover during the day reduces incoming solar irradiation, causing lower daytime temperatures; increased cloud cover during the night traps outgoing longwave irradiation, resulting in warmer nighttime temperatures.

Cooler daytime temperatures may lead to increased heating and energy demand during VRE lull events.

Hydroclimate projections

Climate model projections for rainfall and drought (SMI) show that most of the major hydroelectric dams are situated in locations that are expected to experience decreasing total annual rainfall and soil moisture under a warming climate. This may have implications for the ability of this infrastructure to generate electricity as required. These projections are consistent

with previous research and the general expectation that southeast Australia will become dryer under a warming climate (CSIRO, 2024).

Climate drivers

VRE lull frequency varies from year to year due to natural interannual climate variability. ENSO, IOD and SAM account for a large component of interannual variability across the NEM. During the May-June-July period, La Nina (El Nino) and IOD negative (positive) seasons tend to see an increase (decrease) in solar lulls and compound lulls but do not appear to strongly influence wind lulls.

However, Vincent and Dowdy (2024) have previously found wind lulls over southeast Australia in Autumn and Spring tend to be more frequent during La Nina-like conditions. SAM negative (positive) periods do not strongly influence wind lulls but may slightly decrease (increase) the frequency of solar and compound lulls. This is broadly consistent with Richardson et al. (2023), who found individual REZs and regions could be strongly influenced at seasonal timescales by the main climate drivers, but due to geographical diversity the NEM as a whole was largely resilient.

Synoptic weather during VRE lulls

The synoptic weather associated with VRE lulls can help to explain the climatic drivers of lull events and can also help to identify co-occurring factors which may affect energy demand. Daytime maximum temperatures across most of the NEM, including population centres of Canberra, Sydney and Brisbane tend to be lower than average during solar and compound lulls. Compound lulls occur during the coldest month of the year, so lower than average maximum temperatures during these events may have implications for increased daytime energy demand due to heating.

Wind, solar, and compound lulls all occur with increased cloud cover, especially across the Eastern Seaboard. Increased cloud cover is the primary driver of solar lulls due to its role in blocking incoming solar irradiation. Increased cloud cover during wind lulls is likely to be associated with increased onshore airflow due to more easterly winds, which in most non-coastal locations tend to be weaker than westerly winds. Wind lulls tend to occur when there is a weakening or reversal of the dominant westerly winds over southeastern Australia. This impacts NEM-wide wind resources due to the high concentration of wind REZs across southeast Australia and Tasmania.

Conclusion

The bottom-up approach shows that, under plausible future climate change scenarios, the NEM-wide frequency and duration of VRE lulls are likely to decrease or stay the same. The clearest changes will be for solar lulls which are expected to decrease in frequency and duration. While there is some uncertainty around RCM accuracy, these projections are consistent with the consensus expectation that global warming will cause a poleward expansion and strengthening of the sub-tropical ridge over Australia, leading to clearer skies in many areas (CSIRO, 2024).

Daytime temperatures during compound lulls tend to be cooler than temperatures on non-lull days. Because these events are already occurring during the coldest time of year, there may be implications for VRE lull management due to increased energy demand from daytime heating.

Many of the NEM's largest hydroelectric dams are located in areas that are expected to become dryer in a warming climate. Decreasing rainfall and water availability may have implications for the generation of hydroelectricity.

Climate drivers do influence winds and cloudiness across the NEM at season timescales. In general, solar lulls tend to be more frequent during La Niña and IOD negative periods. However, the NEM spans such a large geographic range that NEM-wide compound lulls are largely resilient to climate driver influences.

Part 2: Top-down Approach

The top-down approach investigates characteristics of individual VRE lull events and their impact on NEM energy production under plausible future climate scenarios with respect to the forecast electricity infrastructure trajectory for 3 time periods (2025, 2030 and 2035).

Weather-based energy traces

Synthetic daily wind and solar energy traces are calculated by calibrating weather data to historical solar and wind traces. Daily weather data representing solar (rsds) and wind ($wind_{150}$) availability are calculated as the area average for each REZ from the observation-based BARRA-C2 (1980-2024) and bias corrected BARPA 7-member ensemble for the SSP126 and SSP370 scenarios (1980-2100).

Historical daily solar and wind traces are obtained from ASL for the 2011 to 2024 period: traces provide a daily value between 0 and 1 representing energy output as a fraction of capacity. For example, a daily wind trace value of 0.5 means that wind power generation on that day is 50% of capacity. Figure 22 shows an example of the close correspondence between daily solar (rsds) and historical trace data at Q2 North Qld Clean Energy Hub.

Synthetic traces are calculated by calibrating daily weather data to daily average wind and solar traces (2011-2024) using quantile mapping. This provides synthetic weather-based daily traces for observed (1980-2024) and modelled future climate (1980-2100) at all relevant REZs (Figure 22). Daily traces can be multiplied by REZ capacity to estimate daily output in GWh from each REZ, and across the NEM. Figure 23 shows benchmarking of synthetic weather-based traces compared to observed output during a severe lull period in 2024—in this example weather-based estimates track closely to observations.

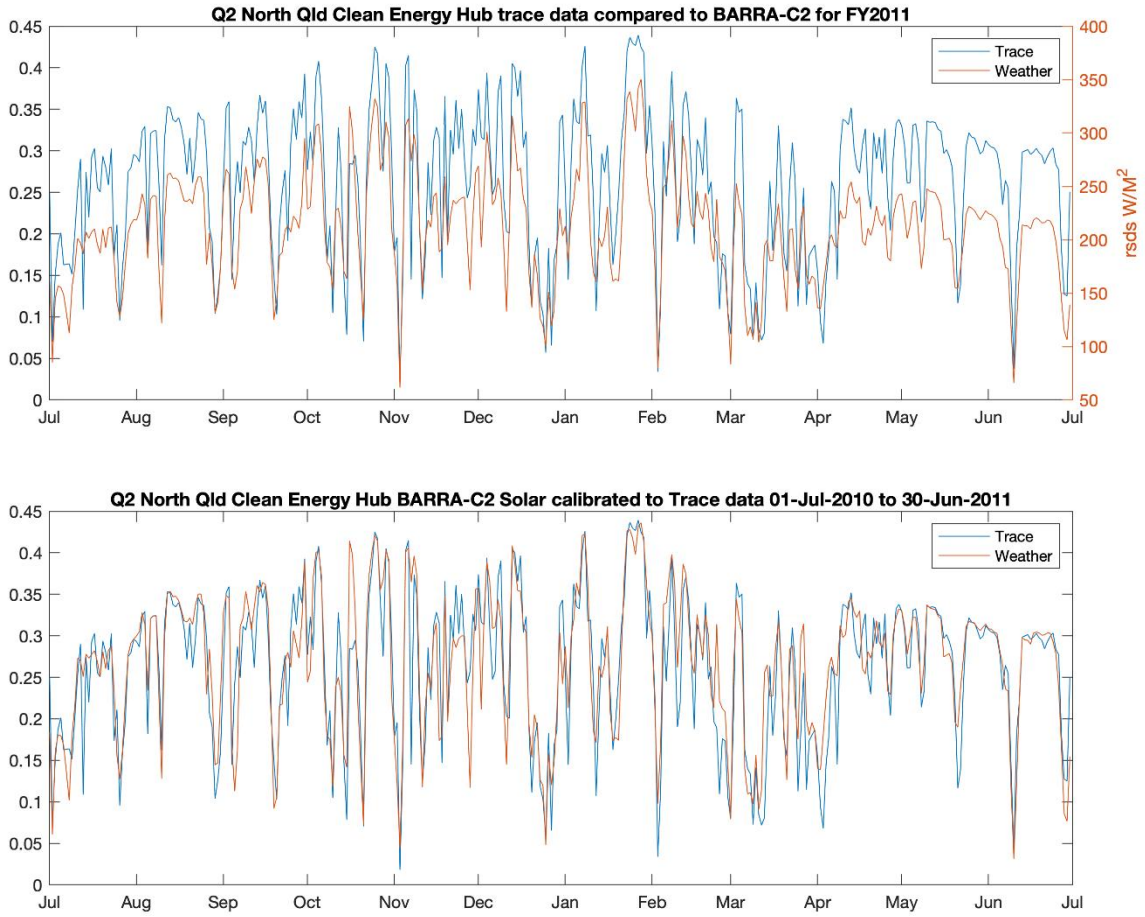

Figure 22 Example showing calibration of daily weather data (rsds) to daily trace data. Top panel shows area averaged rsds in W/m²(orange; right axes) at Q2 North Qld Clean Energy Hub REZ for 2011 compared to historical trace data on a scale of 0-1 (black; left axes) on the same days. Lower panel shows the synthetic weather-based trace (orange) compared to the original trace data, both on a scale of 0-1.

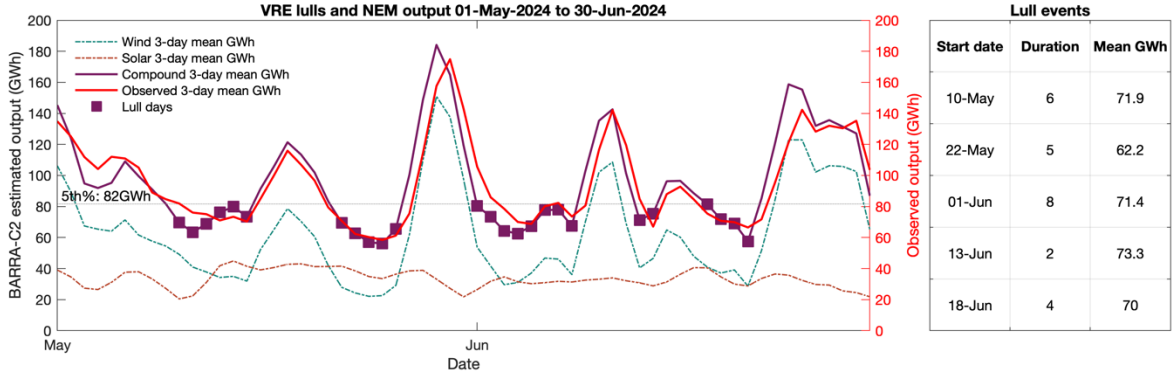

Lull events

Start date	Duration	Mean GWh
10-May	6	71.9
22-May	5	62.2
01-Jun	8	71.4
13-Jun	2	73.3
18-Jun	4	70

Figure 23 Benchmarking events identified from BARRA-C2 compared to severe lulls in 2024. 3-day average $wind_{150}$ and solar (rsds) data are the area average for all included REZs. The compound 3-day mean GWh are the average of all included REZs and have been calculated from the synthetic weather-based trace data by multiplying the daily trace value by REZ capacity. Observed 3-day mean GWh output are shown in red and correspond closely to the weather-based estimate.

Accounting for capacity expansion

Present day REZ capacity and projected expansion in 2045 are shown in Figure 24. For each of the time periods (2025, 2030, and 2035), projected capacity expansion at each REZ is used to calculate daily energy production in MW.

- Daily energy production (MW) = Daily trace value * capacity (MW)

To estimate a total daily NEM-wide weighted capacity factor, total daily NEM energy production is then divided by total NEM capacity.

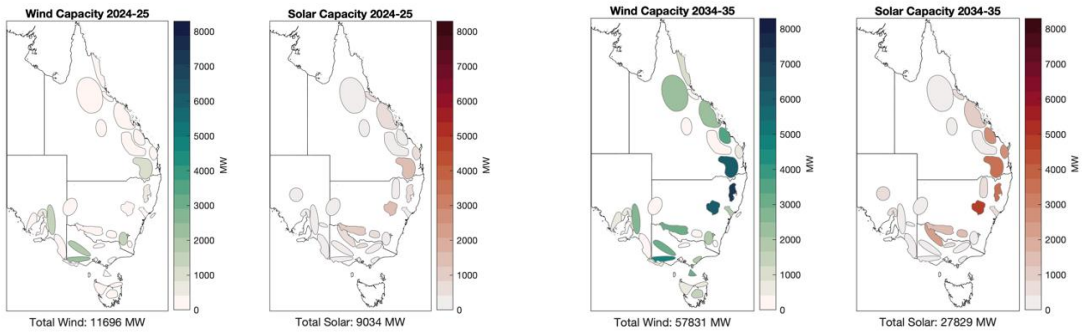

Figure 24 REZ capacity in 2025 compared with projected REZ capacity mix in 2035.

Defining lulls

Lulls are identified as days when the 3-day running average NEM-wide weighted capacity factor is less than the 5th percentile as calculated over the 2000-2023 period (Figure 25). Under present day NEM capacity, the 5th percentile for each of the lull types are: wind 0.18, solar 0.14, and combined 0.19. These values vary slightly between datasets and increase in the future as NEM capacity increases. For consistency the 5th percentile value is held constant at the 2025 value for all future time steps (Figure 25). Lulls events are defined as 1-or-more consecutive lull days separated by non-lull days. Event severity is defined firstly in terms of duration in days, and secondly in terms of event average capacity.

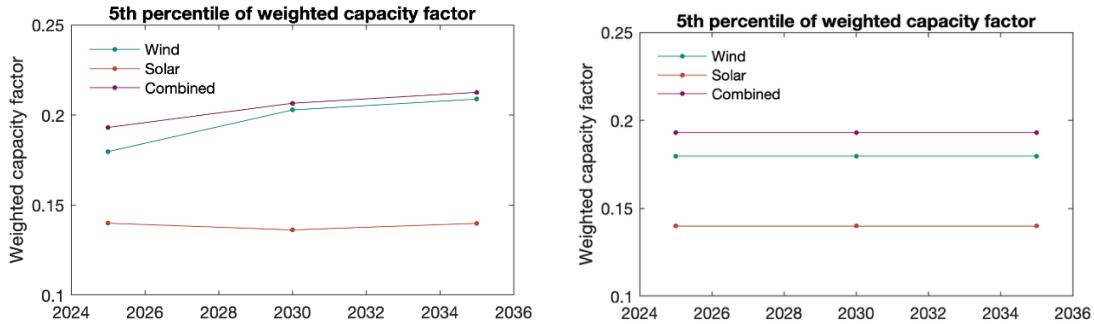

Figure 25 NEM wide 5th percentile weighted capacity factor used as the threshold for defining a lull day under present-day (2025) and future climate, accounting for expected capacity expansion (left panel). Days with NEM-wide weighted capacity factor less than the 5th percentile are defined as lull days. Left panel shows the value of the 5th percentile increases into the future as capacity expands. To understand changes in lulls relative to present-day, the value of the 5th percentiles are held constant at 2025 values (right panel).

Average recurrence intervals

Annual maximum event durations are used to calculate average recurrence intervals (ARI) for each of the 3 time-periods of interest (2025, 2030, and 2035) from a sample of 280 modelled years

(20 modelled years * 7 models * 2 scenarios). In climate modelling it is best practice to sample from a minimum of 20 model years surrounding the year of interest to help account for natural year-to-year variability: for example, in this study, 2025 is represented by model years 2016 to 2035. The BARPA ensemble consists of 7 models and 2 scenarios. For calculation of ARIs we combine 20 modelled years from all models and scenarios to provide a sample of 280 modelled years. In this situation each modelled year can be considered a plausible simulation of the climate system during the time-period. Figure 26 shows an example of ARI calculation for the year 2025 from a sample of 280 modelled years.

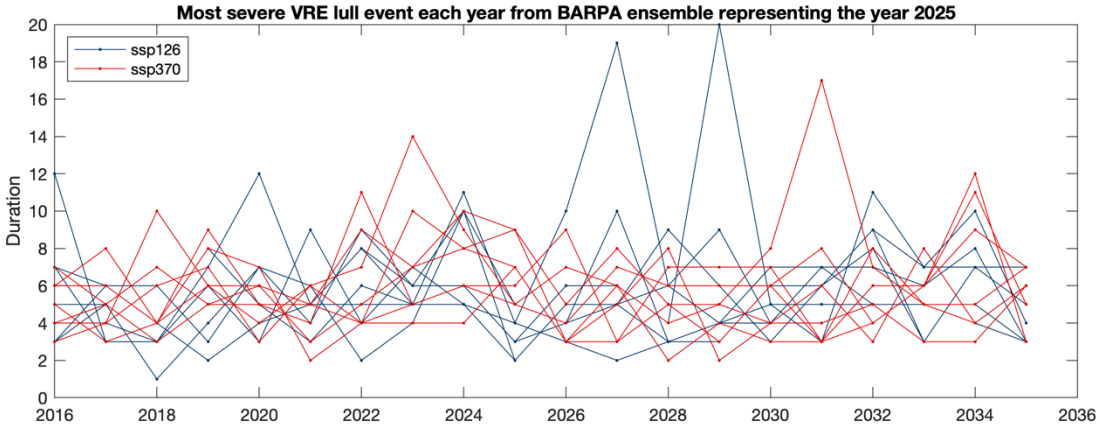

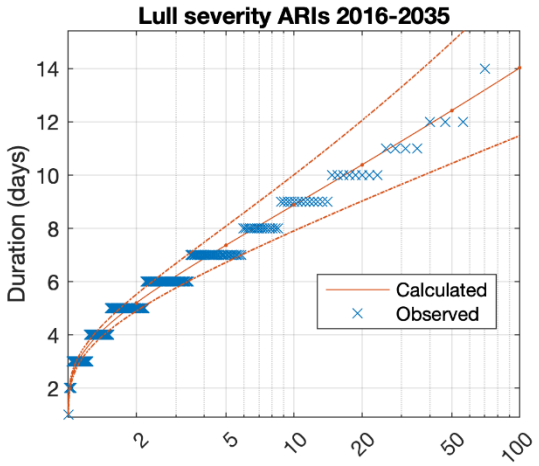

ARIs at various return periods 2016-2035

ARI	Duration (days)
2	5.2
5	7.37
10	8.88
20	10.39
50	12.43

Figure 26 Calculation of average recurrence intervals (ARIs) for annual maximum VRE lull event duration from the BARPA ensemble. Upper panel shows annual maximum event durations for 280 model years between 2016 and 2035 from 7 models and 2 scenarios. This is considered to be a representative of the climate at 2025 and is used to calculate ARIs shown in the lower pannels. Lower left shows the distribution of annual maximum lull duration (blue) and the extreme value fit (orange) used to calculate ARIs shown in the lower right table.

Selection of reference events

Reference events are chosen for 5 severity categories (2-, 5-, 10-, 20-, and 50-year ARIs) as the event with duration nearest the respective ARI: events may be selected from any of the 280 sample years. Where multiple events are identified with the same duration, the reference event is chosen based on the distribution of event average capacity: for example, if event duration is less than the respective ARI then an event of lower average capacity is chosen (Figure 27). Figure 28 shows an example of the reference event chosen to represent a 1-10-year event in 2025.

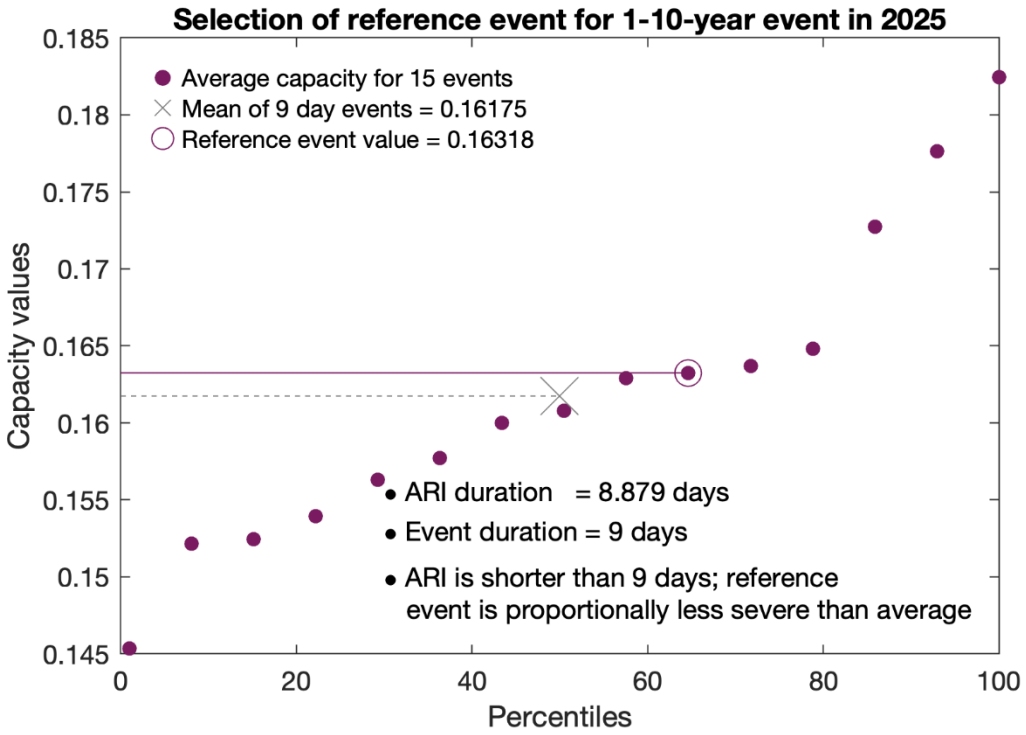

Figure 27 Example of reference event selection for a 1–10-year event in 2025. The extreme value fit shown in Figure 26 gives an event duration of 8.88 days for a 1–10-year ARI. Event durations are measured in whole days and the nearest whole number duration to the ARI is 9 days. The 280-year sample used to represent 2025 contains 15 events with a duration of 9 days. Each of the 15 days has different severity based on event average capacity (shown as a dot for each event). The 1-10-year ARI is shorter than 9 days, so a proportionally less severe (higher capacity) event is chosen as the reference event.

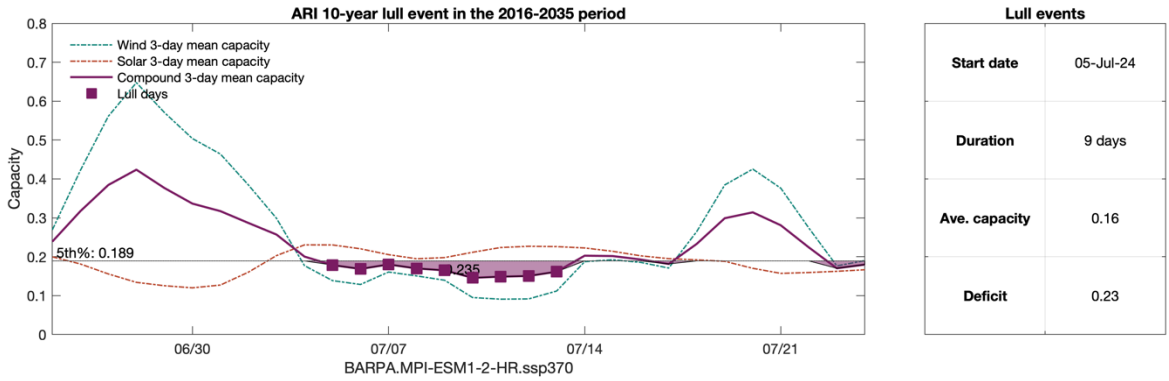

Figure 28 Example of reference event chosen to represent a 1-10-year event in 2025. This event was selected from a sample of 280 modelled years based on event duration and average capacity as illustrated in Figure 26 and Figure 27.

Summary

The top-down approach has identified 30 VRE lull events from RCM projections of plausible future climate scenarios representing a range of recurrence intervals (2-, 5-, 10-, 20-, and 50-year ARIs) and the worst modelled event at time periods (2025, 2030, and 2035). Lulls are defined as periods when NEM wide output is below the 5th percentile; for all future time periods NEM capacity is adjusted to account for expansion under the forecast generation trajectory in the IIO report.

Representative VRE lull event durations range from 4 to 5 days (the 1-in-2-year events) to 9 to 12 days (the 1-in-50-year events), as shown in Table 1. The duration of VRE lulls are forecast to

decrease across the 20-year time horizon of the development pathway. This may be due to the forecast increased diversity of VRE across the NEM, particularly for wind whereby different locations tend to have complimentary generation profiles. The decrease is also consistent with projections for a decrease in VRE lull frequency and durations shown in Part 1. Note that whilst the lull duration may decrease, the impact on the electricity system may be larger if there is a greater reliance on renewables.

For the next stage of the analysis, the 30 representative VRE lull events are simulated in time-sequential modelling by ASL to assess the resilience of the development pathway.

Table 1 Duration of VRE lulls at varying recurrence intervals for present day (2025-26) and future time periods

Lull duration (days)	1-in-2-year event	1-in-5-year event	1-in-10-year event	1-in-20-year event	1-in-50-year event
2025-26	5	7	9	10	12
2029-30	4	6	7	8	10
2034-35	4	5	6	7	9

Appendix 1

Previous IIO report approaches to VRE lull assessment

Table 2 Recap of the 2022 IIO report

	Use of climate modelling	Definition of VRE lulls	Resilience assessment
Summary	• **Historical dataset**: the 42-year ERA5 dataset, utilising analysis conducted by OECC and UNSW.	• **Duration below a threshold**: lulls defined separately across wind/solar and each NSW REZ, then coincidence lulls analysed. • This resulted in 1-to-4-day VRE lull events.	• **Simplified post-processing:** using outputs of time sequential modelling. • VRE lulls extended to reflect historical data. • Demand was increased to reflect the known correlation with VRE lulls.
Key limitations	• Did not capture the potential impact of climate change.	• Binary nature of threshold definition may not capture the worst lull events.	• Simplified post-processing did not capture half-hourly dispatch dynamics.

Table 3 Recap of the 2023 IIO report

	Use of climate modelling	Definition of VRE lulls	Resilience assessment
Summary	• **Historical dataset:** the 43-year MERRA-2 dataset, analysed with support from Endgame Economics.	• **Severity over a fixed time threshold**: Minimum NSW generation availability over pre-defined 1-day, 3-day and 7-day durations. • This resulted in a 7-day VRE lull with 13% VRE capacity factor.	• **Time-sequential modelling** • VRE lulls were scaled to reflect historical data.
Key limitations	• Did not capture the potential impact of climate change.		• Demand was not further increased • The profile of the historical VRE lull was not captured

Appendix 2

Future Climate Modelling

The best available information on Earth's future climate comes from numerical climate models. Climate models use equations that represent physical processes controlling weather and climate to simulate how Earth's climate system might respond to increasing greenhouse gas concentrations.

Global climate modelling is usually conducted within frameworks established by the World Climate Research Programme (WCRP). The WCRP itself was established in 1980 by the World Meteorological Organization (WMO), which is a specialized agency of the United Nations. Some of the main modelling projects established by the WCRP include the Coupled Model Intercomparison Project (CMIP) and the Coordinated Regional Downscaling Project (CORDEX).

These frameworks ensure that model simulations produced by the world's climate modelling research groups are developed in such a way that data can be shared and evaluated. Most of the output from these projects is freely available for commercial use.

The model outputs from CMIP are used directly in the United Nations Intergovernmental Panel on Climate Change (IPCC) assessment reports and are the primary evidence base for projections of future climate change. The latest iteration of CMIP is phase 6, which commenced in 2013, and model outputs started to become available from 2020. Planning for CMIP7 is currently in its early stages, with initial outputs not expected until around 2027.

CMIP Scenarios

Greenhouse gas emissions are driven primarily by human activities. Therefore, future warming levels will depend mostly on the socioeconomic behaviour of Earth's population. Because future socioeconomic behaviour is unknown, climate models simulate a range of possible scenarios, from best-case scenarios where greenhouse gas emissions are rapidly reduced and the magnitude of warming is small, to worst-case scenarios where emissions continue to increase and catastrophic warming beyond 4°C above pre-industrial (1850-1900) occurs by the end of the century.

There are currently two sets of scenarios commonly used in climate modelling: CMIP5 Representative Concentration Pathways (RCP) and CMIP6 Shared Socioeconomic Pathways (SSPs). RCP scenarios from CMIP5 are currently being superseded for most applications by SSP scenarios. Global warming levels associate with the Tier-1 SSP scenarios are shown in Figure 29:

- SSP1-26—Unlikely future with warming of 1.7 ± 0.6 °C and some adaptation challenges
- SSP2-45—Most likely future with warming of 2.7 ± 1.3 °C and significant adaptation challenges
- SSP3-70—Possible future with warming of 3.9± 1.1 °C and difficult adaptation challenges
- SSP5-85—Unlikely future with warming of 4.7 ± 2.6 °C and limited adaptation options

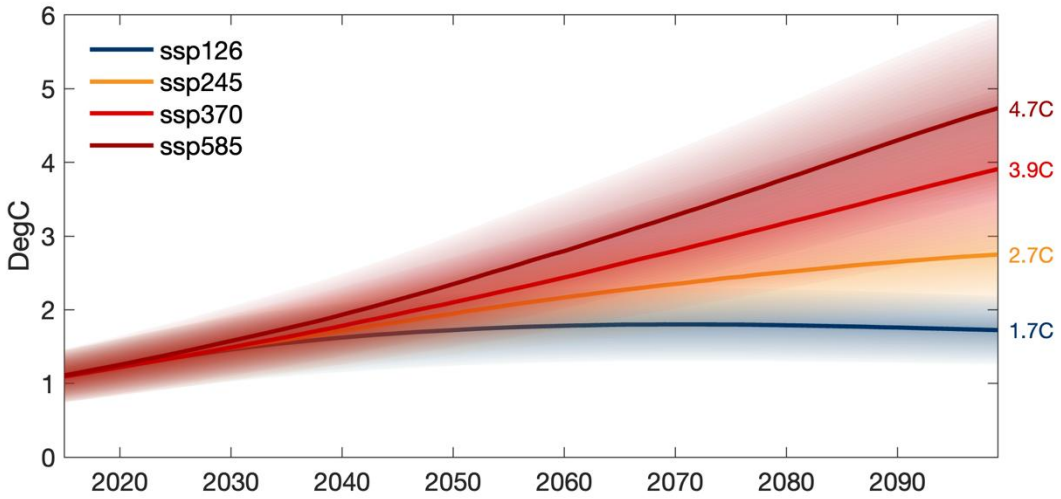

Figure 29 Global mean temperature increases relative to pre-industrial (1850-1900) under the Tier-1 SSP scenarios (data from IPCC 2021).

Regional Climate Modelling for Australia

Outputs from global climate models are of limited use without bias correction and regional downscaling. Global climate models used in CMIP attempt to simulate a wide range of earth system processes so are computationally expensive. To manage the computational costs, model grid resolutions are typically coarse, around 50km to 100km. At these resolutions, large-scale processes, such as global temperature change, and synoptic weather systems are reasonably well-simulated, but locally relevant processes, such as winds, orographic rainfall, and mesoscale storms are not. Climate models also tend to have systematic biases, whereby variables such as temperature or wind are slightly different from observations at a given location. To account for these limitations, climate model output usually needs to be downscaled, and/or bias-corrected prior to use.

Downscaling adapts global climate model output to a finer resolution more suitable for understanding local scale processes. There are three main approaches to downscaling: statistical, dynamical, or machine learning:

1. Machine learning approaches—currently under development and have not yet been successfully applied to future climate data (eg, Rampal et al., 2024)
2. Dynamical downscaling—involves running high resolution weather models and is usually conducted within the CORDEX framework. Due to the high computation demands, regional climate models are usually only run over limited spatial domains. CMIP6 SSP scenarios are becoming available throughout 2024 and 2025.
3. Statistical downscaling—relatively computationally efficient and provides results comparable to output from regional climate models, with some caveats, such as that small-scale storms are not well simulated. Statistical downscaling has the advantage that data are also bias corrected.

Regional climate modelling of the Australian domain (AUS) is conducted by several international research organisations and four main Australian research groups: CSIRO, University of Queensland (UQ), the Bureau of Meteorology, and the University of New South Wales (UNSW)/ NSW and Australian Regional Climate Modelling (NARCliM). These groups have previously

published CMIP5 based RCP scenario simulations and are in the process of publishing a selection of SSP scenario simulations throughout 2024 and 2025:

- BOM: BARPA
- CSIRO: CCAM
- UQ: CCAM
- NARCliM2: WRF

In 2021 the Electricity Sector Climate Information project (ESCI, 2021) comprehensively evaluated Australian-produced regional climate model simulations of RCP4.5 and RCP8.5 and recommended a set of 4 bias corrected regional/ global climate model combinations (CCAM-GFDL-ESM2M, CCAM-NORESM1-M, BARPA-ACCESS1-0, and NARCliMJ-CANESM2) as the most suitable ensemble for projections associated with rainfall, temperature, and Forest Fire Danger Index (FFDI). A similar evaluation has not yet been undertaken for the latest generation of SSP based regional climate model simulations, so it is currently not known how well these models perform, or which models should be selected for the optimum ensemble.

Regional climate models used in this study

Two regional climate model ensembles were considered for use in this study: NARCliM2.0 and BARPA (NCI 2024). NARCliM2.0 was the preferred ensemble, however the Department of Climate Change, Energy, the Environment and Water (DCCEEW) team advised that the required wind variables, u150m and v150m would not be available in time for this project. The BARPA ensemble was therefore selected for use in this project.

The BARPA regional climate model ensemble consists of 2 scenarios and 7 driving models: ACCESS-CM2, ACCESS-ESM1-5, CESM2, CMCC-ESM2, EC-Earth3, MPI-ESM1-2-HR, and NorESM2-MM.

Bias Correction

Global and regional climate model simulations usually contain small biases which need to be corrected prior to these data being used for risk assessments. Bias correction uses observational data spanning a period overlapping the model data as a target to adjust model values, so they better represent observations. For most applications bias correction is a necessary data processing step. Bias correction also downscales the model data to the same spatial resolution as the observational data and, in many cases, can be effectively applied in place of regional climate modelling.

A collaborative research project is currently underway to evaluate a range of downscaling and bias correction methods (Vogel et al., 2023). The ESCI project used a method called Quantile Mapping for Extremes (QME), which is one of the best performing bias correction approaches (Vogel et al., 2023) and is described in Dowdy (2023).

All regional climate model data used in this report has been bias corrected by Risk Frontiers using interpolation and QME. Figure 30, 33, 34, and 35 below illustrate the bias correction process showing biases in the original BARPA data and the reduction in bias and increase in spatial resolution after QME correction is applied.

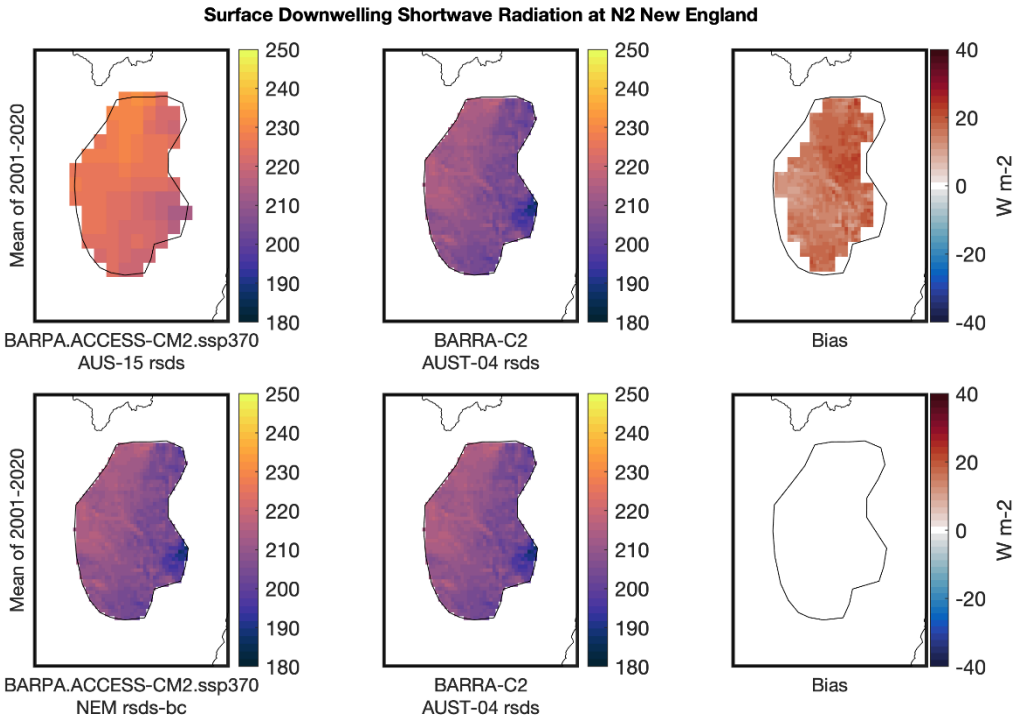

Figure 30 Bias correction of BARPA regional climate model simulation of rsds from the ACCESS-CM2 model to BARRA-C2. Upper-left panel shows time-averaged mean rsds from the BARPA-ACCESS-CM2 simulation at 17km resolution and the upper-centre panel shows equivalent rsds from the BARRA-C2 reanalysis at ~4km resolution. The upper-right panel shows bias (difference) between BARPA-ACCESS-CM2 and BARRA-C2. Lower-left panel shows bias correction of BARPA-ACCESS-CM2 to BARRA-C2 and lower right panel shows reduced bias after correction.

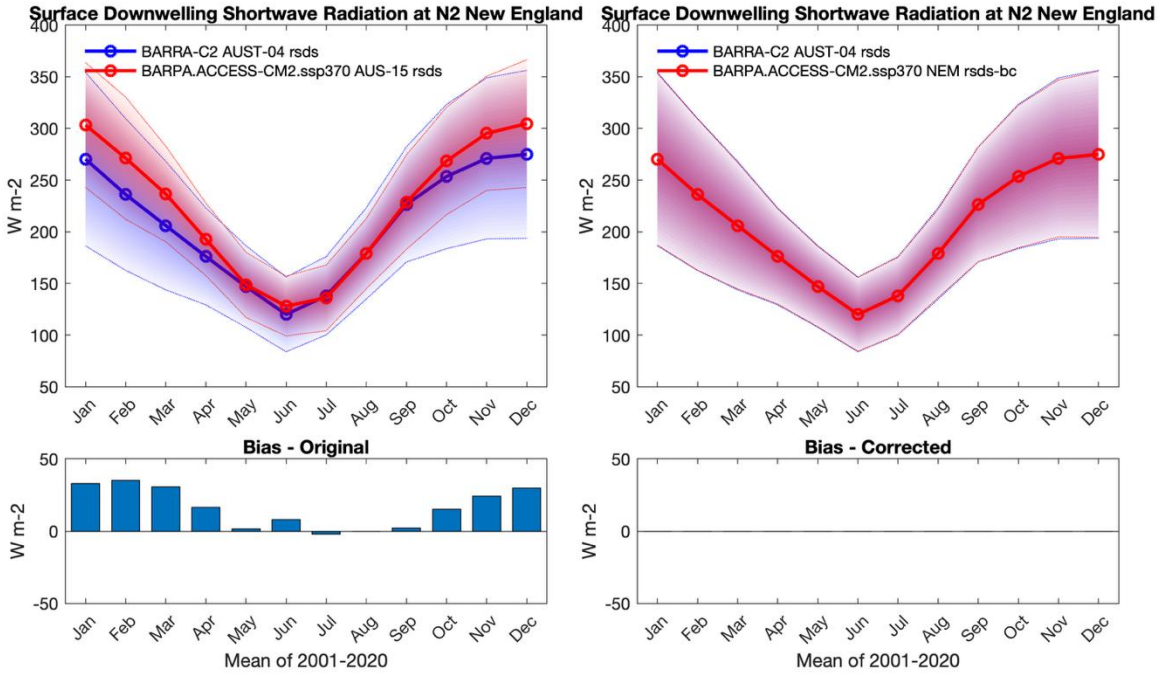

Figure 31 Bias correction of BARPA-ACCESS-CM2 rsds to BARRA-C2 rsds. Left panels show mean monthly bias between the model and observational data. In this example the strongest positive bias is during the summer months, and there is minimal bias during August. Right panel shows differences have been mostly removed after bias correction.

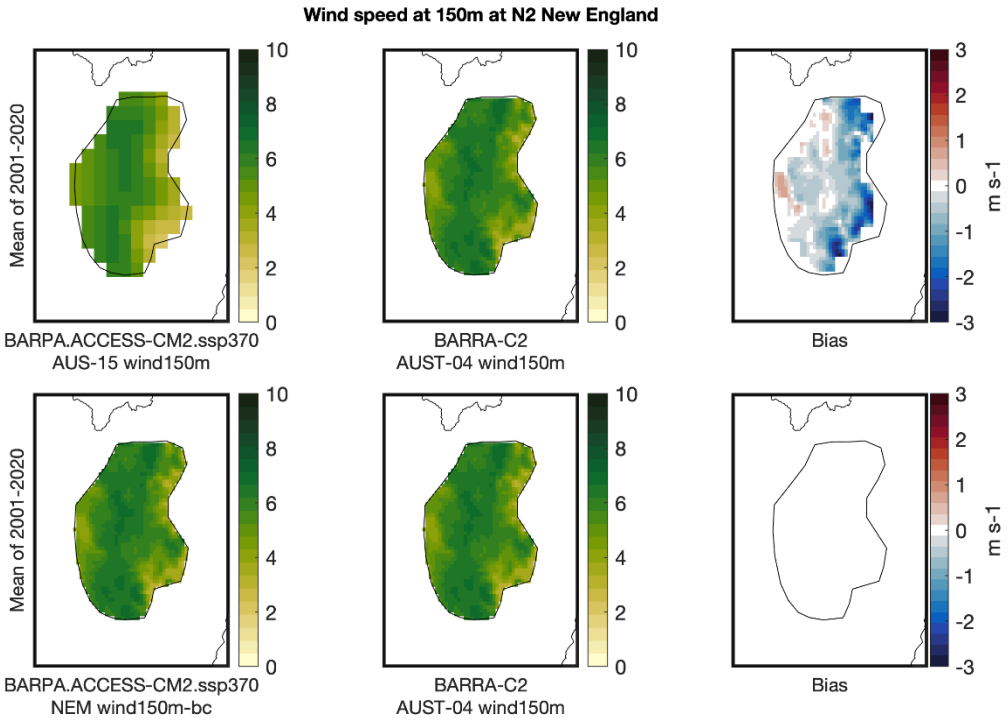

Figure 32 Bias correction of BARPA regional climate model simulation of wind150m from the ACCESS-CM2 model to BARRA-C2. Upper-left panel shows time-averaged mean wind150m from the BARPA-ACCESS-CM2 simulation at ~15km resolution and the upper-centre panel shows equivalent wind150m from the BARRA-C2 reanalysis at ~4km resolution. The upper-right panel shows bias (difference) between BARPA-ACCESS-CM2 and BARRA-C2. Lower-left panel shows bias correction of BARPA-ACCESS-CM2 to BARRA-C2 and lower right panel shows reduced bias after correction.

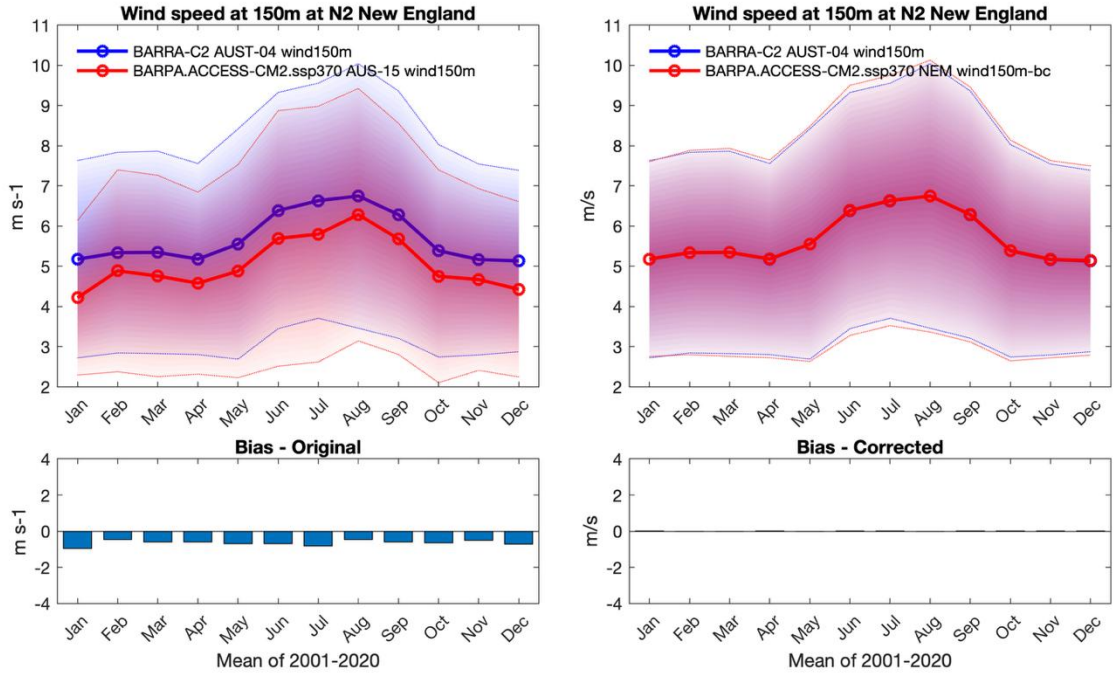

Figure 33 Bias correction of BARPA-ACCESS-CM2 wind150m to BARRA-C2 wind150m. Left panels show mean monthly bias between the model and observational data. In this example negative biases are seen during most months. Right panel shows differences have been mostly removed after bias correction.

Uncertainty in climate modelling

Regional climate models (RCMs) used in this report are decision support tools that can help plan for an uncertain future. However, RCM simulations encompass a range of uncertainties that should be considered. These include, but are not limited to:

- Uncertainties around future emission scenarios which depend on global energy and land use policies. These are addressed by simulating multiple plausible scenarios; in this study SSP126 and SSP370 scenarios have been used.
- Uncertainties in global climate model (GCMs) representation of large-scale climatic changes. RCMs are "driven" by GCM simulations. Possible uncertainties due to GCMs are partially addressed by including simulations from an ensemble of RCM simulations driven by seven different GCMs.
- Uncertainties in the representation of internal climate variability such as the El Niño Southern Oscillation (ENSO). There is considerable uncertainty in GCM representation of internal climate drivers such as ENSO, and uncertainty as to how these may vary under a warmer climate. While this is partially addressed by considering output from an ensemble of different models, it remains one of the biggest uncertainties in climate model-based projections for Australia (e.g., Browning et al., 2024).
- Uncertainties in bias correction can impact the final values obtained from RCM simulations. Bias correction is an important, but complex step in adjusting RCM simulations for potential bias by comparing them to observational based data. While Risk Frontiers have used one of the best performing methodologies, bias correction is imperfect and remains an area of active research (e.g., Vogel et al., 2023).
- Uncertainties in the interpretation of RCM simulations can often arise due to over interpretation of model precision. RCM simulations do not provide accurate forecasts for future climate. They are designed to simulate a range of possible futures; in this project they are interpreted within the context of a distribution of values and associated uncertainty.

Despite the uncertainties listed above, RCMs are the best tools available for understanding how global warming may affect regional climate. See Abramowitz et al (2024) for more information on climate model uncertainties.

References

Abramowitz et al. (2024). Working with Uncertainty in Climate Planning and Adaptation. UNSW institute for Climate Risk and Response. https://climateextremes.org.au/wp-content/uploads/Uncertainty-Briefing-Note-DIGITAL.pdf

Browning et al. (2024). How a climate conundrum at the heart of the Pacific is challenging disaster preparedness in Australia. Risk Frontiers Briefing Note. https://riskfrontiers.com/insights/how-a-climate-conundrum-at-the-heart-of-the-pacific-is-challenging-disaster-preparedness-in-australia/

CSIRO (2024). State of the Climate Report 2024. https://www.csiro.au/en/research/environmental-impacts/climate-change/State-of-the-Climate

Dowdy, A. (2023). A bias correction method designed for weather and climate extremes. http://www.bom.gov.au/research/publications/researchreports/BRR-087.pdf

ESCI (2021). ESCI Project Final Report. https://www.climatechangeinaustralia.gov.au/en/projects/esci/

Hunt, E. D., K. G. Hubbard, D. A. Wilhite, T. J. Arkebauer, and A. L. Dutcher. (2009). The development and evaluation of a soil moisture index. *Int. J. Clim.*, **29**, 747–759, https://doi.org/10.1002/joc.1749.

IPCC (2021). Summary for policymakers. In: *Climate change 2021: the physical science basis. Contribution of Working Group I to the Sixth Assessment Report of the Intergovernmental Panel on Climate Change*. https://www.ipcc.ch/report/ar6/wg1/downloads/report/IPCC_AR6_WGI_SPM.pdf.

OECC (2023). *Lulls in variable renewable energy sources*. Office of Energy and Climate Change, https://www.energy.nsw.gov.au/sites/default/files/2023-05/NSW_OECC_Lulls_in_variable_renewable_energy_sources_202302.pdf.

Rampal, N., P. B. Gibson, S. Sherwood, G. Abramowitz, and S. Hobeichi. (2024) A Robust Generative Adversarial Network Approach for Climate Downscaling and Weather Generation. https://doi.org/10.22541/essoar.171352077.78968815/v1.

Richardson, D., A. J. Pitman and N. N. Ridder. (2023). Climate influence on compound solar and wind droughts in Australia. *npj Clim. Atmos. Sci.*, **6**, 184, https://doi.org/10.1038/s41612-023-00507-y.

Su, Chun-Hsu et. al. (2022). BARPA: New development of ACCESS-based regional climate modelling for Australian Climate Service. Bureau of Meteorology (Bureau Research Report - 069), Retrieved from http://www.bom.gov.au/research/publications/researchreports/BRR-069.pdf

Su, Chun-Hsu et. al. (2022) BARRA2: Development of the next-generation Australian regional atmospheric reanalysis (Bureau Research Report - 067), Bureau of Meteorology, Retrieved from http://www.bom.gov.au/research/publications/researchreports/BRR-067.pdf

Vogel, E. and coauthors. (2023). An evaluation framework for downscaling and bias correction in climate change impact studies. *J. Hydrol.*, **622**, 129693, https://doi.org/10.1016/j.jhydrol.2023.129693.